ELECTROCHEMICAL SEPARATION AND DETECTION OF CHEMICAL SPECIES
IN FLOW CELL: EXAMINATION OF A MICROFLUIDIC DEVICE

by

Sean J. Park
A Thesis
Submitted to the
Graduate Faculty
of
George Mason University
in Partial Fulfilment of
The Requirements for the Degree
of
Master of Science
Chemistry & Electroanalytical Chemistry

Committee:

_____   Dr. Abul Hussam, Thesis Director

_____   Dr. John Schreifels, Committee Member

_____   Dr. Hao Jing, Committee Member

_____   Dr. Benoit Van Aken, Graduate
                                     Coordinator

_____   Dr. Gerald Weatherspoon, Department
                                     Chairperson

_____   Dr. Donna M. Fox, Associate Dean,
                                     Office of Student Affairs & Special
                                     Programs, College of Science

_____   Dr. Peggy Agouris, Dean, College of
                                     Science

Date: _____   Spring Semester 2019
                                     George Mason University
                                     Fairfax, VA

Electrochemical Separation and Detection of Chemical Species in Flow Cell: Examination of a Microfluidic Device

A thesis submitted in partial fulfillment of the requirements for the degree of Master of Science at George Mason University

By

Sean Park
Bachelor of Arts
George Mason University, 2016

Director: Abul Hussam, Professor
Center for Clean Water and Sustainable Technologies
Department of Chemistry and Biochemistry

Spring Semester 2019
George Mason University
Fairfax, VA

Dedication

I dedicate my work to my fiancé Bohyun Kim who has been supportive, encouraging and continually providing moral, spiritual, and emotionally support.

Acknowledgements

       I gratefully acknowledge the support and guidance from my thesis advisor Dr. Hussam. Without his thoughtful encouragement and careful supervision, this thesis would never have taken shape. His provision of an excellent lab environment also helped tremendously to execute and finish the research.

       I would also like to give a special thanks to Dr. Shim in Busan, Korea for giving me an opportunity to work with his findings as well as providing me a device to work with.

Table of Contents

List of Tables

List of Figures

List of Equations

Abstract

ELECTROCHEMICAL SEPARATION AND DETECTION OF CHEMICAL SPECIES
IN FLOW CELL: EXAMINATION OF A MICROFLUIDIC DEVICE

Sean J. Park, M.S.

George Mason University, 2019

Dissertation Director: Dr. Abul Hussam.

The development of microscale devices or "Lab-on-a-Chip" has intrigued
widespread interest due to its possible analytical applications in the field of medical,
environmental, and material science. For example, microscale flow cells exhibit great
surface-to-volume ratio and therefore provide a high sensitivity even from a weak surface
interaction. Furthermore, different configurations of flow cells deliver their specific
electrochemical properties used for analyzing the electroactive species. The detection of
redox species is commonly practiced and comprehended however, the separation by
electrochemical field is not well understood. In order to better understand the separation
phenomenon with the microfluidic channel, a simple wall jet flow cell has been tested.
Then, the results obtained from these experiments were used to design experiments where
separation and detection can be done on the same platform. The <u>electrochemical potential
modulated microchannel (EPMM)</u> is the device capable of separating and detecting
electroactive species on the same platform. Both EPMM and wall jet flow cell were used

in this research to determine the area of the electrodes, diffusion properties, time constant, and other electrochemical analysis with $K_3Fe(CN)_6$ and metal ions. Various analytical parameters such as scan rate, flow rate, and concentrations also helped on characterizing the system. As a result, 2.5mM $K_3Fe(CN)_6$ flowing at 4μL/min to the system and scanned at different rates determined the area of an electrode and the diffusion coefficient to be $(1.00\pm0.05) \times 10^{-3}cm^2$ and $(8.05\pm0.3) \times 10^{-6}cm^2/s$, respectively. Several plots were constructed with the observed electrochemical parameters and confirmed the system is quasireversible. The plots also determined the detection limits as 0.1mM for concentration and 0.14nA for current. Furthermore, the electron transfer rate constant was found to be $(5.52\pm0.04) \times 10^{-3}cm/s$. Besides the basic voltammetric properties of the cell and the redox couple, the detection of metal ions was attempted at a ppb level using the EPMM device in addition with the AC modulation voltage and frequency. In effect of electrolysis on detecting the metal ions with AC modulation of 1.0V and 1.0MHz, there were at least seven distinctive peaks correspondent to the metal ions with respect to their retention order. The detection limit of 0.20 - 1.15ppb and the sensitivity level of 50 - 250nA/ppb showed possibilities of enhancement.

1.0 Introduction

Chemical separation and detection on the same platform integrated into a single device is the new trend in analytical chemistry. Separation techniques such as microfiltration, high efficiency distillation, and chromatography had been the typical way of separating analyte from a relatively simple mixture before the trend.[1,2] As newly introduced chemical species exhibited more complex and diverse properties, advanced analytical separation techniques, such as GC-MS and LC-MS were then developed and introduced for different fields of researches.[2] The applications of gas chromatography, high-pressure liquid chromatography, and capillary electrophoresis were especially useful due to their extensive and excellent separation efficiency for complex mixtures. However, these are bulky and expensive instruments meant for the laboratory environments with appropriate facilities to maintain them.[20] Because "small is beautiful," the present trend in analytical chemistry is the development of miniaturized systems known as the "lab-on-a-chip" where separation and detection are integrated into one unit.[1,22] lab-on-a-chip had also expanded its scientific usage and the researchers are generating more versatile and compacted versions based on microfluidic system.[3,4,5] These different designs of lab-on-a-chip include wall jet, tubular, parallel-planar, and perpendicular-planar and they provide different quantitative analysis.[8] Nonetheless, these devices are now being frequently used in fields such as medical, environmental, and material science.[1]

The start of this small scaled technology emerged in the late 1970 with the development of silicon technology for machining mechanical microdevices, which later came to be known as microelectromechanical system (MEMS). MEMS is a process technology with both mechanical and electrical components integrated on a micro-scaled device.[31,32] Microfluidics is a subset of MEMS where both are referred to as microdevices or lab-on-a-chip and follow the standard procedures of fabrication: patterning, photolithography, and etching etc.[33] The significance of these devices is the capability to perform multiple lab functions that are integrated into a single circuit. Microfluidics especially deal with behavior, precise control, and manipulation of fluids that are very small scaled to provide as much information with a smaller power input than the older macroscopic circuits with bigger components.[1] Because of this trend, not only has microfluidics been growing in popularity in multiple fields, but also showed potentials to replace some of the major instruments that are presently being used, such as the ICP-MS.[2]

An application of electrochemical methodology to the microfluidic channel not only detects, but also separates samples. Although selective retention of species based on preferential molecular interactions as in chromatography is capable of separating chemical species, the lack of portability and long measuring time have favored the microfluidic channel.[2,3,6] The microfluidic channel, specifically the EPMM device is known to have advantages of small volume samples, short analysis time, and high efficiency.[1] The EPMM device is also acknowledged for successfully demonstrating the separation and detection of electroactive species. It has been shown that the separation

and detection of multiple trace metals at a very low concentration with this microfluidic channels is possible under optimal conditions.[2,4] The efficiency of separation was further improved upon the effect of electrophoresis and electro-osmosis, which both phenomena involve motion of particles and liquids affected by electric field.[1,16] Thereafter, reliability and reproducibility examination using real life samples were analyzed. This particular experiment concluded that reliability and reproducibility of the EPMM device is not an issue unlike the other microfluidics. These outcomes supported the advantages of the EPMM device and also proved some of the common disadvantages of microfluidics invalid. Yoon stated that these powerful features of the EPMM device could replace some of the old separation methods.[2] In order to validate the results, a critical evaluation of the microfluidic channel will be performed in addition to exploring the potential applications for examining complex redox species.

2.0 Purpose

The purpose of the work is to characterize flow cells for detection of electroactive species utilizing various electrochemical techniques. One specific purpose is to examine the EPMM device for the separation of trace metals. This device has not been commonly utilized in electrochemical analysis and the phenomenon has not been explicitly understood. The primary goal of this research is to evaluate the different types of flow cells, observe the effect of applied AC potentials on separation, and understand the mechanism.

3.0 Overview of electrochemical techniques

This section describes the electrochemical techniques used for quantitative chemical analysis on microfluidic channels. Electroactive and redox species are also studied using these electroanalytical methods. The techniques can mainly be categorized into three sections depending on which aspects of the cell are being controlled or measured. The three main categories are voltammetry, potentiometry, and coulometry.

Voltammetry measures current while constant potential is applied to the electrode surface. Furthermore, voltammetry uses three electrode system, working, counter, and reference electrode, to measure the resulting current. This method is commonly used to identify the reduction potential of an analyte and its electrochemical activity. A superclass of voltammetry, amperometry, also measures current but as a function of time or potential. Potential here, however, is held constant unlike varying the potential applied to the electrode.

Coulometry is a technique where a current or potential is applied to electrolytically convert the oxidation states of an analyte. Coulometry thus measures the total current passed in respect to total charge passed or electrons passed. Therefore, knowing the oxidation state and electrons passed can determine the concentration of the analyte or vice versa.

3.1. Cyclic voltammetry (CV)

Cyclic voltammetry (CV) is one of the powerful electrochemical technique for study of species with electroactive and redox characteristics. CV is a technique where electron-transfer reaction can be induced in solution for redox species. Mass-transfer also plays a significant role in CV at the electrode surface which is controlled by the scan rate and either one of the mass transport modes: convection, migration, and diffusion.[8,20-24] The movement of the analyte by convection involves mechanical force, migration involves electrical field, and diffusion involves concentration gradient.[7]

The redox reaction is examined electrochemically by driving electrons along the system to measure the change in current as a function of potential at a fixed rate.[23] The initial potential and the vertex potential are important parameters in this technique. The initial potential should ideally equal to the final potential if the redox couple is reversible. Therefore, the oxidation reaction will be represented during forward scan and the reduction reaction thereafter. The positive and negative values of the parameters are a matter of convention and a general diagram of the CV is as shown in Figure 1.
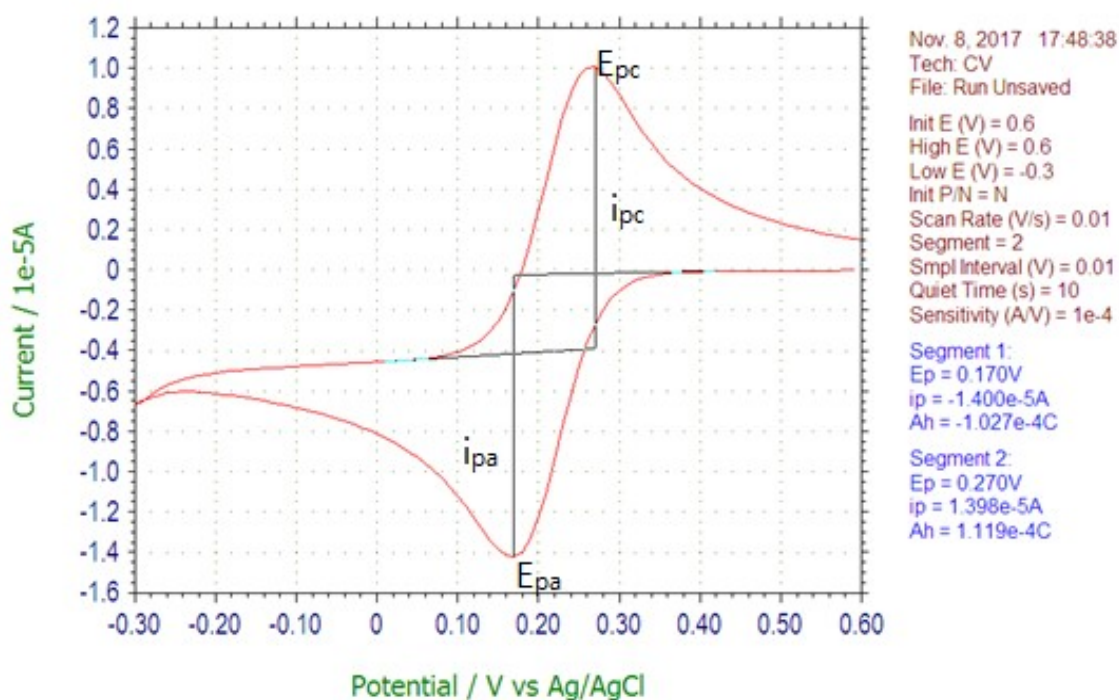
Figure 1. A Cyclic voltammogram of a ferricyanide, $[Fe(CN)_6]^{3-}$ ions in aqueous solution at 10mV/s scan rate. Experimental conditions and results E_{pc}, E_{pa}, i_{pc}, and i_{pa} are displayed on the right.[27]

The shape characterization in CV needs to consider the role of mass transfer as well as electron transfer of the species at the surface of an electrode simultaneously. The reduction current becomes zero when there is no electron transfer, which is achieved by the excitation potential. In contrast, decreasing the potential will increase the current and reach the maximum current expressed by i_{pc}, cathodic peak current. A similar mechanism is applied for i_{pa}, anodic peak current, exhibited by an oxidation and reversed current. The other two parameters are the cathodic and anodic peak potentials and these fundamental parameters are used to further characterize the redox properties. The Randles-Sevcik

equation expresses a reversible reaction utilizing the obtained variables and constants as shown in equation 1.

$$i_p = 2.69 \times 10^5 n^{3/2} A D^{1/2} C v^{1/2} \tag{1}$$

The parameter values obtained experimentally can be applied in the equation where i_p is the peak current in Ampere (i_{pc}-i_{pa}), n is the electron stoichiometry, A is the area of the electrode in cm^2, D is the diffusion coefficient of the species in cm^2/s, C is the concentration of the species in mol/cm^3, and v is the scan rate in volts/s. Additionally, the number of electron stoichiometry should reflect on peak potentials as expressed by equation 2 in an ideal situation of reversible reaction. The ratio of peak current should be a unity and equal to approximately 1 as well.

$$\Delta E = |E_{pc} - E_{pa}| = 0.0591/n \tag{2}$$

In this work, the treatment and modeling of the analyte demonstrated the mechanisms of each mass transport mode by using different types of flow cells. Furthermore, potassium ferricyanide, $K_3Fe(CN)_6$, was used as an analyte because the redox couple ferricyanide/ferrocyanide, $[Fe(CN)_6]^{3-}/[Fe(CN)_6]^{4-}$ displays quasireversible and steady-state voltammograms under specific conditions. As a result, $K_3Fe(CN)_6$ is expected to have a linear relationship between the peak currents to the square root of scan rate and directly proportional to the concentration as described by the Randle-Sevcik equation.

3.2 Anodic Stripping Voltammetry (ASV)

Anodic stripping voltammetry (ASV) is an instrumental technique used to measure the concentration of metal ions in solutions.[25,26] ASV is performed in a two-step process of deposition and stripping. The first step is where the metal ion is deposited on the electrode at a potential where the reaction is diffusion controlled and reduced to metal-amalgam. Then the metal ion from metal-amalgam is oxidized back (or stripped off) into the solution by applying an opposite potential ramp. For example, $Pb^{2+} + 2e^- + Hg(l) \rightleftharpoons Pb(Hg)$ is the deposition process, then $Pb(Hg) \rightleftharpoons Pb^{2+} + 2e^- + Hg(l)$ is the stripping process.[8] While oxidation continues, the current is measured as a function of potential and the peak potential will identify the metal ion whereas the peak current will be used to measure the concentration of the ion. The current-potential profile is then used to measure $W_{1/2}$, the width of the peak at half height, in order to calculate n, the degree of reversibility of the reaction, using equation 3.

$$W_{1/2} = 3.52\ RT/nF \tag{3}$$

The principle behind deposition process relies on holding the deposition potential constant far from the standard reduction potential of the redox couple. The concentration of the deposited species will reflect on the deposition time as well. As a result, a significant concentration of the species will accumulate in the mercury film as amalgam $(M(Hg))$.[8,27]

Though this technique is used to measure the unknown concentrations of the metal ion by constructing a calibration curve, another implementation of current as a

function of known concentrations calibration curve can contribute as part of the optimization process of specific metal ions.

3.3 Chronoamperometry (CA)

Chronoamperometry (CA) examines metal complex redox couple such as $[Fe(CN)_6]^{3-}$ and $[Fe(CN)_6]^{4-}$ (ferrocyanide) to characterize their electrochemical properties. CA is a technique where double potential step is applied to obtain signals. These two excitation steps correspond to reduction and oxidation of the redox couple resulting in i-t response (current-time). Furthermore, the responses are affected by the potential range and overall electron transfer reaction of the redox couple.[28] The initial potential is chosen at a point of no electron transfer interaction while the final potential is where the reaction is completely diffusion controlled, a potential far from the equilibrium potential.[27,29,30] These two parameters can be determined from either linear scan voltammetry (LSV) or CV.

In this research, CV technique was used to determine the potential range for CA. A typical CV scan of a standard $[Fe(CN)_6]^{3-}$ analyte at a millimolar concentration and a fixed scan rate exhibits two major peaks. These two peaks represent anodic and cathodic currents where the rate of electron transfer is at maximum and the reaction approaches a diffusion-controlled limit. At the start of the scan where the current is nearly zero, the corresponding potential will be selected as the initial potential of CA since there is no electron transfer as mentioned.

In CA technique, a plot of i(A) as a function of 1/square root of t(s), using the Cottrell's equation (4), can be drawn to calculate the area of the electrode considering other variables are accurately known.

$$i(t) = nFAD_o^{1/2}C_o/(\pi t)^{1/2} \qquad (4)$$

The equation is expressed as a function time where n is the number of electrons, F is the Faraday's constant, A is the area of the electrode, D_o is the diffusion coefficient, and C_o is the bulk concentration.

A series of resistors and capacitors can also characterize the electrode and solution interface of an electrochemical cell containing only the supporting electrolyte. Such an electrical network can be studied by applying a short pulse at a known duration and measuring the change in current as a function of time between two electrodes as if it is a low pass filter. The i-t response for such a low pass filter is expressed by

$$\ln[i(t)] = \ln(E/R_s) - t/\tau \qquad (5)$$

where R_s is the solution resistance, C_d is the double-layer capacity of the working electrode, τ is the time constant of the cell which is equal to R_sC_d, and E is the voltage step.[27] In an electrochemical cell containing only the supporting electrolyte, supposedly the non-Faradaic process, the electrodes are typically categorized as 'ideal polarized electrode (IPE),[8] in which no charge transfer occurs across the electrode-electrolyte interface. Although no real electrode behaves as an IPE over the given potential range for a solution, some electrode-electrolyte system presumably approaches the idealized polarizability over limited potential range.[1,8] The purpose of looking into the double-layer capacity and charging current is because of its significance in measuring the total current,

especially for low faradaic currents as well as in IPE system. However, even the non-Faradaic currents will have some contributions from the charging current at certain values of R_s and C_d which are represented by the solution resistance and the double layer at the electrode interface respectively. Furthermore, IPE system does not allow charges to cross its electrode interface when the potential is changed.[17-19] As such, the behavior of the electrode-solution system was compared with a capacitor, governed by the integrated form of equation 5; $q = EC$ where q is the charge stored on the capacitor in coulombs, E is the potential across the capacitor in volts, and C is the capacitance in farads.[8] This equation will be explained in later sections.

4.0 Materials and methods

4.1 Materials

Potassium ferricyanide, $K_3Fe(CN)_6$ (Mallinckrodt, maximum 0.05% Ferro compound, 0.01% Chloride, 0.005% insoluble matter, and 0.01% Sulfate impurities) samples were prepared by a series of dilutions. A 10.02mM stock sample was first prepared by mixing 0.3299g of solid $K_3Fe(CN)_6$ with 100.0mL ultra-pure 18MΩ DI water. Then a series of dilutions were performed to prepare 5.00mM, 2.50mM, and 1.25mM $K_3Fe(CN)_6$ into 50.0mL volumetric flasks. The analyte was then filtered out with a 0.25-micron nylon filtration tip and kept under dark, dry area to prevent photo oxidation. The heavy metal ions (100ppb each Co, Cd, Cr, Pb, and Se, and 300ppb each Fe and As) analyte sample was obtained as the stock reagent prepared from respective nitrate salts in 0.10M hydrochloric acid, HCl. The supporting electrolyte (SE) 100.0mM potassium chloride, KCl, was prepared by dissolving 1.4910g of solid KCl (Sigma-Aldrich), with 200.00mL of ultra-pure 18MΩ DI water. A 0.1M acetate buffer (4.53pH) was made by diluting 17.4M glacial acetic acid (CH_3COOH) into a 100.0 mL volumetric flask and adding drops of 0.1M HCl until the designated pH was reached.

4.2 Instruments

The electrochemical analysis such as cyclic voltammograms (CV), Chronoamperogram (CA), linear scan voltammogram (LSV), anodic stripping

voltammetry (ASV) and square wave voltammograms (SWV) were performed with the electrochemical analyzer (CHI Inc, Texas, USA) along with the CHI1220B software. An automated syringe pump (KdScientific Instrument model # 220, Massachusetts, USA) was used to inject supporting electrolyte continuously through the electrode cell. Two different types of the syringes (Precision Sampling Corp and National Scientific, Massachusetts, USA) and the flow tube (Cole-Parmer Instrument Company, Illinois, USA) with inner diameter of 0.01inch were used for delivering samples to the electrode cell. A more precise 2.0mL glass syringe (Precision Sampling Corp) was used in the syringe pump to avoid bending of the plunger. A 6-port injection valve (Upchurch Scientific, V-450, California, USA) was also used to load and inject analyte while the supporting electrolyte was continuously flowing. The tube was cut in different sizes for 6-port injection valve, in which the loading loop tube consisted of 3.84±0.01inches with a volume of 4.94±0.01μL and the flow tube consisted of 5.91±0.01inches with a volume of 7.60±0.01μL. Therefore, the total dead volume was 12.54±0.01μL. The sinusoidal AC potentials of different frequencies were generated by a waveform generator (KkMoon, Dual Channel Dds Signal Generator/Counter, MHS-5200A, China) to alternating AC electric field to the chip electrode.

5.0 Result and discussion

Multiple electrochemical techniques were used to characterize two different flow cell systems. Utilizing a particular electroactive species, both flow cells successfully presented electrochemical properties that enabled further calculations for the characterization of flow cells. The results from a simply constructed wall jet flow cell were compiled to analyze various unknown parameters of the cell electrode as well as the flow cell itself. Those determined parameters were then employed to a designated equation to compare the calculated values with the literature values. As such, the properties shown from the thin-layer electrochemical cell correlated to that of the typical flow cells.

The experiments with thin-layer electrochemical cell were necessary before evaluating a more compact and versatile microfluidic device called electrochemical potential modulated microchannel (EPMM). Using the same electroactive species, $[Fe(CN)_6]^{3-}$, a series of experiments were performed to reproduce what the device is capable of doing: separating and detecting trace metal ions. In the EPMM device, the application of AC induced field established opposite electrical fields at a high frequency, i.e. electrophoretic field, that affected the electrochemical properties of redox species. After completing the analyses of both flow cells and redox species, the experiment

further progressed into detecting and perhaps separating the trace metal ions with the same device.

5.1 The thin-layer electrochemical cell

5.1.1 The apparatus set up of the thin-layer cell

In an attempt to understand the electrochemical flow cell systems, two different microfluidic systems were assembled, tested, and evaluated. The first flow cell was made of two acrylics blocks (72.71 x 69.65 x 6.32 ± 0.01 mm) assembled with screw-bolts. The thin-layer cell (12.99 x 50.45 x 0.62 ± 0.01 mm) is sandwiched between these blocks as shown in Figure 2. This electrochemical cell is a commercial (CHI Inc) chip electrode consisting of three electrodes: working electrode, counter electrode, and a Ag/AgCl reference electrode printed on a PVC plastic sheet. A rubber o-ring was placed in between the blocks (and electrochemical cell) as a flow channel and two holes were drilled as an injection and ejection ports just like a wall jet cell geometry. Flow tubes were then inserted and hot-glued to about 0.1inch holes to drive the pressured flow in and out (arrows) of the electrode cell as shown in Figure 2 (without the flow tubes).
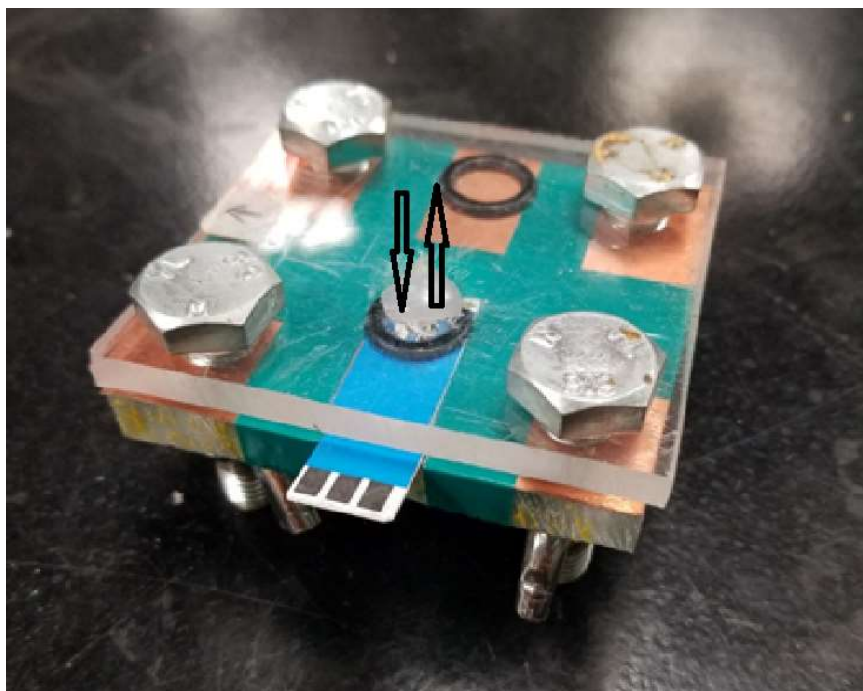
Figure 2. A photograph of the thin-layer flow cell made in the lab. The electrode connection tabs (black) are used to connect working, reference, and counter electrode leads. The epoxy Cu-sheet underneath the cell was used as a Faraday's shield to reduce noise. The o-ring thickness (height) was 1.30±0.01mm and its inner and outer diameter was determined to be 14.50±0.01mm and 17.5±0.01mm, respectively. The gap between two acrylics was determined to be 1.75±0.01mm. The volume of the flow cell was then calculated to be 0.215±0.001mL.

The supporting electrolyte was in a continuous flow system while the analyte was manually loaded and injected with a 6-port injection valve. The flow rate of the syringe pump was calibrated by collecting a known volume of water at a fixed flow rate and comparing the mass to that of the volume. The flow rate precision (RSD) error was < 1% ($\pm 0.0091 mm^3$/min standard deviation). A general scheme of the experimental set up is shown in Figure 3.
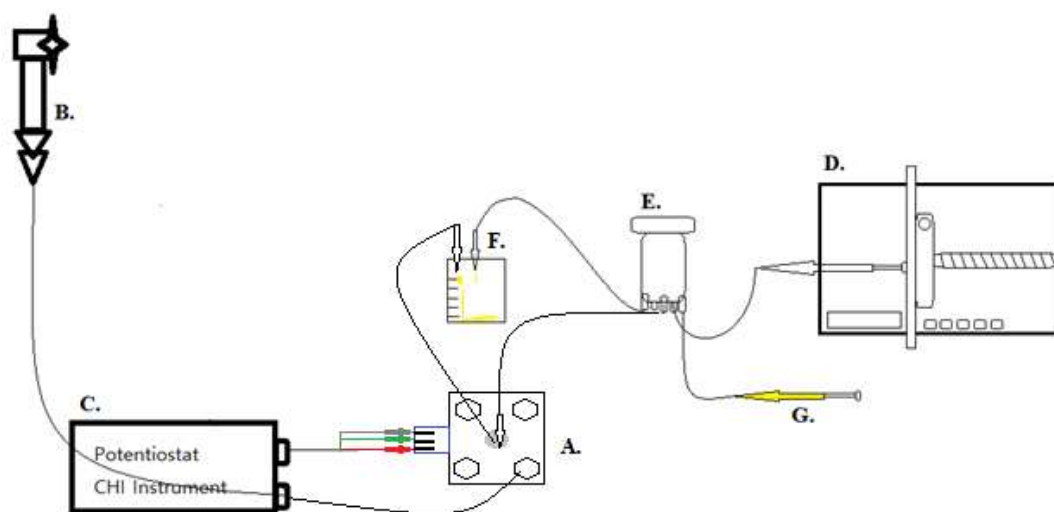
Figure 3. General scheme of the thin-layer cell apparatus. **A.** the thin-layer electrochemical cell with the chip electrode sandwiched, **B.** a metal faucet as electrical grounding and attached to the potentiostat and one of the screw bolts, **C.** the potentiostat, **D.** automated syringed pump, **E.** 6-way injection port, **F.** waste container, and **G.** analyte syringe.

Multiple electrochemical analyses of $[Fe(CN)_6]^{3-}$ were performed using various techniques such as CV, CA, and ASV. Different parameters were examined to observe the effects and determine electrochemical properties of the system. The CHI1220B program was mainly used throughout the experiments and it ran by parameter inputs depending on the analysis technique. The outputs were then the automatic recognition of the peak currents and peak positions (respect to peak potential). The instrumental parameters included level of gains, scan rate, potential range, amplitude, frequency, sensitivity, and pulse width (measuring time) like shown in the general CV diagram (Figure 1).

5.1.2 Characterization of the thin-layer cell

As depicted in Table 1, scan rates influence electrochemical responses. CV accounts for redox species and uses the technique of electron-transfer reaction in solution to analytically study the species. Mass-transfer also plays a significant role in CV at the electrode surface which is controlled by the scan rate. $[Fe(CN)_6]^{3-}$ and $[Fe(CN)_6]^{4-}$ (ferrocyanide) displayed quasireversible and steady-state voltammograms under specific conditions and by its behavior of simultaneous oxidation and reduction with respect to scan rate as expressed by the Randles-Sevcik equation and the data collected.

Table 1. Data from CV experiment with the first flow cell with 2.5mM $[Fe(III)(CN)_6]^{3-}$ in quite solution. The subscripts pc and pa refer to cathodic plot and anodic plot respectively. SR is an abbreviation for scan rate. Initial and high E(V) = 0.5, Low E(V) = -0.1, sample interval(V) = 0.001, and sensitivity(A/V) = 0.001. The processed data are as listed, and formula as indicated. The electron stoichiometry, n, was calculated by $0.0591/\Delta E$, from equation 2.

SR (V/S)	Epc (V)	Epa (V)	ipc (A)	ipa (A)	SQRT (SR (V/s^(1/2)))	ΔE=|Epc-Epa| (V)	E°=(Epc+Epa)/2 (V)	ipc/ipa	n	ln(ipc) (A)	Epc-E° (V)
0.01	0.170	0.270	-1.400E-05	1.398E-05	0.100	0.100	0.220	-1.001	0.591	-11.18	-0.050
0.03	0.150	0.280	-2.208E-05	2.197E-05	0.173	0.130	0.215	-1.005	0.455	-10.72	-0.065
0.05	0.170	0.280	-2.932E-05	2.900E-05	0.224	0.110	0.225	-1.011	0.537	-10.44	-0.055
0.10	0.130	0.300	-3.472E-05	3.328E-05	0.316	0.170	0.215	-1.043	0.348	-10.27	-0.085
0.20	0.110	0.320	-4.358E-05	3.874E-05	0.447	0.210	0.215	-1.125	0.281	-10.04	-0.105
0.50	0.070	0.350	-5.318E-05	4.244E-05	0.707	0.280	0.210	-1.253	0.211	-9.842	-0.140
1.00	0.028	0.375	-8.820E-05	6.000E-05	1.00	0.347	0.202	-1.470	0.170	-9.336	-0.174
2.00	-0.005	0.399	-1.161E-04	6.637E-05	1.41	0.404	0.197	-1.749	0.146	-9.061	-0.202
5.00	-0.062	0.434	-1.570E-04	6.587E-05	2.24	0.496	0.186	-2.383	0.119	-8.759	-0.248
Avg:						0.250	0.209		0.318		

The volume of the cell was first calculated using the cylinder volume calculation, $\pi r^2 h$, and resulted in $20.87mm^3$ or $208.7\pm0.1\mu L$. The area of the electrode was then calculated from a series of CV experiments where the peak current was measured as a function of square-root of the scan rate according to Randles-Sevcik equation. Table 1 shows the data collections from the CV experiments as well as the process data to determine the electrochemical reversibility. By plotting i_{pc} and i_{pa} vs. SQRT(SR) (square-root of scan rate) as shown in Figure 4, the slope of the cathodic plot and literature value of diffusion coefficient reduction, D_R, $6.32 \times 10^{-6}\, cm^2/s$, were used to calculate the area of the electrode which was $(1.00\pm0.05) \times 10^{-3}\, cm^2$. The electrochemical reversibility was then analyzed using the previously determined area of an electrode plus the slope of the anodic plot. The diffusion coefficient oxidation, D_o, calculated was $(8.05\pm0.3) \times 10^{-6}\, cm^2/s$. Furthermore, the value of D_o was confirmed by Cottrell, absolute method referenced by S. J. Konopka and Bruce McDuffle[9] averaging about $8.14 \times 10^{-6}\, cm^2/s$. The similarities in these values suggested that the system is quasireversible as shown below.
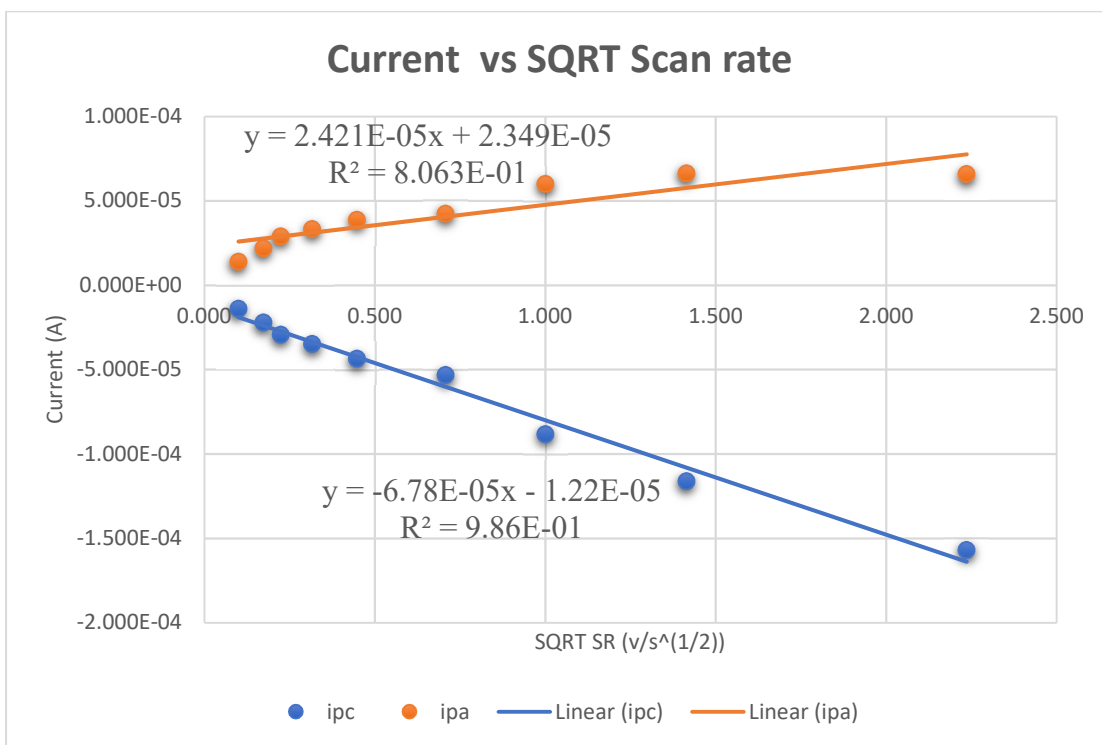
Figure 4. Plot of ipc and ipa vs. (scan rate)$^{1/2}$ from the processed data in Table 1. Utilizing the Randles-Sevcik equation, the area of the electrode can be computed as well as the diffusion coefficient using either one of the redox reactions, vice versa. The series are as indicated where orange color represents anodic plot and blue is cathodic plot. Anodic plot: $Y = ((2.42\pm0.4) \times 10^{-5}) X + (2.35\pm0.4) \times 10^{-5}$ and $R^2=0.81$. Cathodic plot: $Y = ((-6.78\pm0.3) \times 10^{-5}) X - (1.22\pm0.3) \times 10^{-5}$ and $R^2 = 0.99$.

Another characteristic of a quasireversible system with stable product is that the values of i_{pc} and i_{pa} should ideally be the same, and thus giving an absolute ratio of one. Table 1 confirmed and provided ratios close to one at slower scan rates. However, when scan rates were considerably faster, the absolute ratios began to increase. This relationship can be explained by the behavior of electron transfer to analyte molecules or diffusion limited current. As the scan rate is increasing, the peak potentials are moving farther from the E^0, making electron transfer more favorable as defined by the diffusion

controlled reaction. Furthermore, the electrodes can behave similar to a Nernstian system where the electron transfer between an electrode and a redox species is fast with less current flowing. This phenomenon is depicted in Table 1 where the peak currents are lower at slower scan rates and therefore achieving the complete Nernstian system.[7]

In an ideal reaction of $[Fe(CN)_6]^{3-}$ and $[Fe(CN)_6]^{4-}$, the number of electrons transferred is determined to be one. According to equation 2 ($\Delta E = |E_{pc}-E_{pa}| = 0.0591/n$), one electron process should exhibit a potential of 59.1mV. With the fast electron transfer in a quasireversible reaction, the value of ΔE should not exceed 59.1mV. This is illustrated by Figure 5 where ΔE increased as scan rate increased. Then, as scan rate is further increased, the ΔE value seemed to hinge as if the maximum potential is approaching. This mechanism is indicated by equation 2 where ΔE at an even faster scan rate, the value of ΔE will be less than or equal to 59.1mV. However, if the scan rate reaches the higher point where electron transfer is slow in quasi or irreversible reaction, the ΔE value will increase in excess of 59.1mV and result in kinetically controlled reaction.
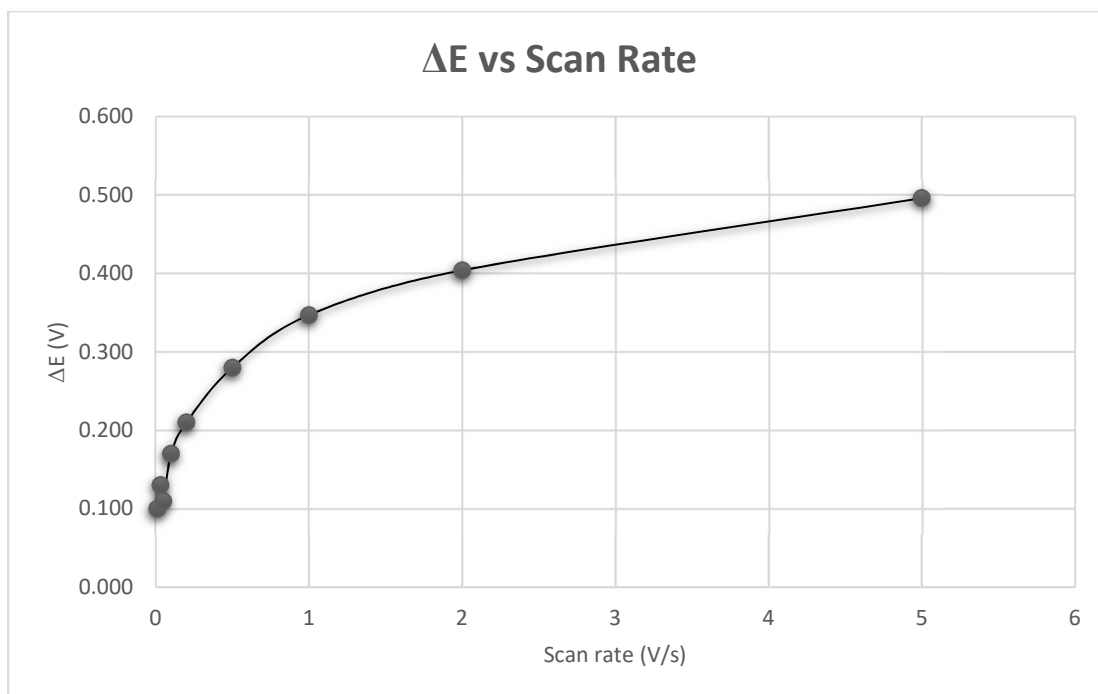
Figure 5. Plot of ΔE(V) vs scan rate (V/s) from the process data in Table 1. The graph was constructed in order to observe the effect of scan rate on ΔE, which can be calculated by subtracting cathodic potentials by anodic potentials in an absolute value. The coordinates are as indicated from Table 1.

One of the characteristics of a completely reversible reaction is that the peak potentials do not change as a function of scan rates. This is because the electron transfer rate is so fast that the peak potential is determined solely by diffusion of the analyte. In contrast, an irreversible system relies on the electron transfer rate constant, because the scan rate is proportional to the electron transfer rate; faster the scan rate, longer the concentration gradient takes to react to the ΔE. Furthermore, the literature value of E^0 for this redox couple is 200mV vs. Ag/AgCl reference electrode. Table 1 confirmed this number by averaging all the E^0 respect to scan rates, verifying that the system is quasi-irreversible.

More quantitative characteristics were performed using the Butler-Volmer equation

$$i_{pc} = 0.277nFACk_se^{(-\alpha NF/RT)(Epc-Eo)} \tag{6}$$

where α is the symmetry of the potential energy barrier of the transition state, N is the number of electrons in the rate determining step of the reaction, F is the Faraday constant (96485 coulomb/equiv.), R is the gas constant, T is the absolute temperature (F/RT=38.92V), and k_s is the electron transfer rate constant in cm/s. Using an algebraic relationship of current and potential, a plot of $\ln(i_{pc})$ vs. $E_{pc}-E^o$ was constructed to determine the constants as illustrated in Figure 6.
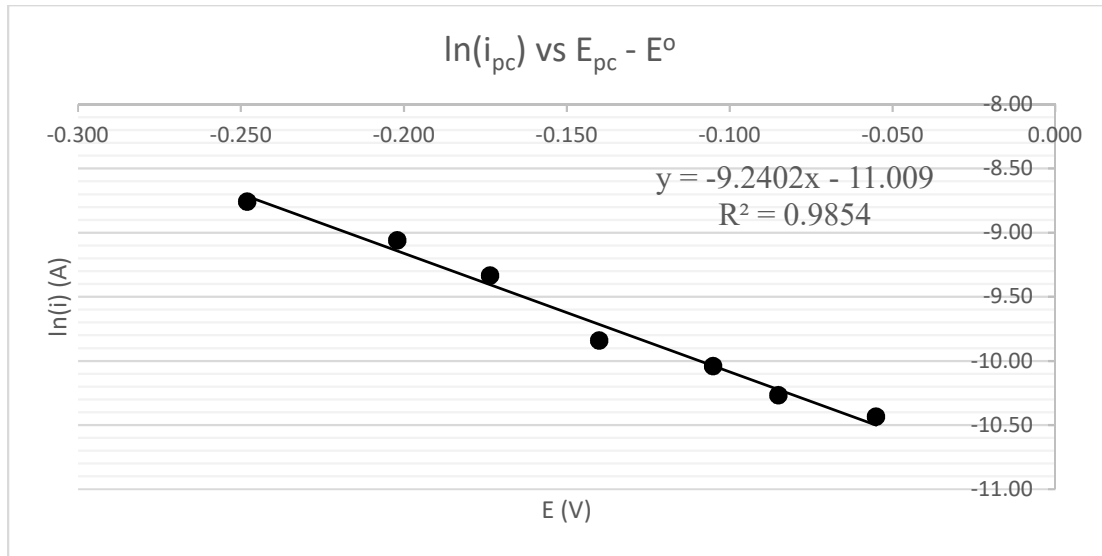
Figure 6. Plot of $\ln(i_{pc})$ (A) vs. $E_{pc}-E^o$ (V) from the process data in Table 1. In order to determine the the symmetry of the potential energy barrier of the transition state, the number of electrons in the rate determining step of the reaction, and the electron transfer rate of the redox species and electrode, this plot was drawn. The best linear fit line was drawn to be y = (-10.895±1)x – (11.32±0.2) with R^2 of 0.9362 initially. However, after the two outlier plots were omitted, (-0.050,-11.18) and (-0.065,-10.72), a new trend line was established, y = (-9.2402±0.5)x – (11.009±0.08) with R^2 of 0.9854.

The slope represents ($-\alpha NF/RT$) in which F/RT is already expressed as 38.92V. Dividing each term with the slope led to a value 0.2374 ± 0.01 which equals to the potential energy barrier of the transition state. The other left-over terms were represented by the y-intercept value, -11.01 ± 0.08, that enabled the calculation of k_s. Dividing the exp(intercept) value with constants plus the area of the electrode resulted in k_s equal to (5.52 ± 0.08) x 10^{-3}cm/s, which is the electron transfer rate constant at a given area that was previously determined. This was also confirmed by S. J. Konopka and Bruce McDuffle[9] where the values averaged (5.41 ± 0.15) x 10^{-3}cm/s with 0.10M KCl medium. However, it has been said that the results by electrochemical methods may differ experimentally by 10%-20%.[9] Nonetheless, the similarities in values once again verified that the same redox couple behaves similarly irrespective of the cell geometry.

Different concentrations of the analyte were tested to observe the relevance in terms of currents. The concentration calibration curve shown in Figure 7 exhibits a linear relationship between current(μA) and concentration(mM) as expressed in the Randles-Sevcik equation. The linearity was confirmed with the R^2 value of 0.9928 and a best fit line of $y = (2.21\pm0.1)x + (0.38\pm0.8)$. The standard errors were calculated using the LINEST function and analyzed the detection limit as 0.8μA or 0.1mM. The plot errors presented also verified that the concentrations of solution had an inverse relationship with the detection limit, which is the lowest quantity (current or concentration) of $[Fe(CN)_6]^{3-}$ solution that can be distinguished in a blank value. As a result, 2.5mM $[Fe(CN)_6]^{3-}$ was selected for optimal concentration for further investigation.
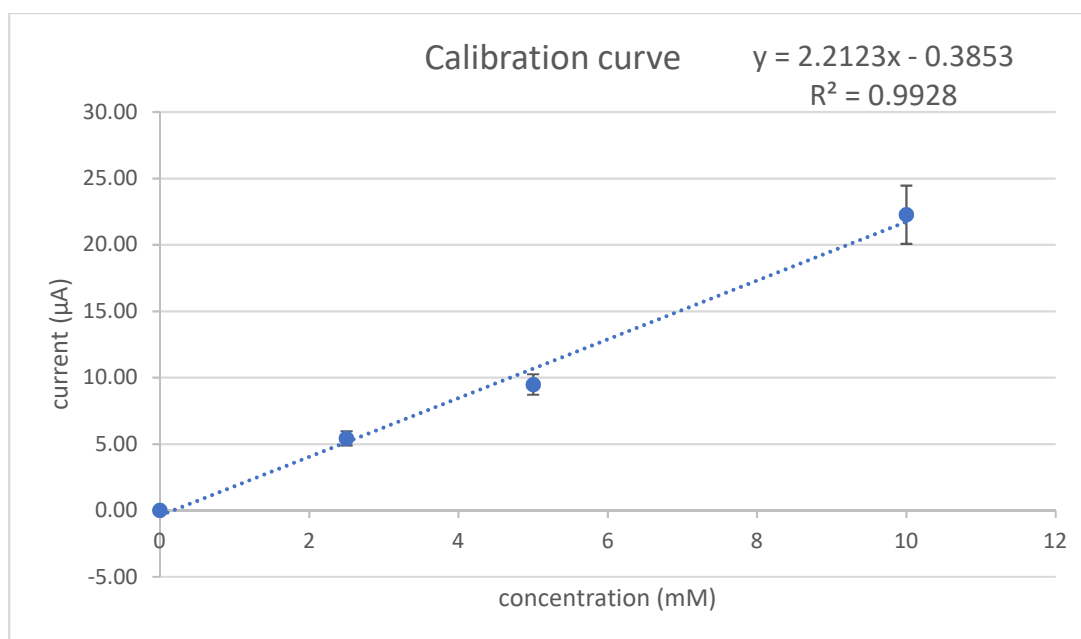
Figure 7. A calibration curve of the $[Fe(III)(CN)_6]^{3-}$ in thin-layer cell. The concentrations range from 10mM, 5mM, and 2.5mM from a series of dilution and currents were recorded accordingly. The error bars of $\pm$ 2.2, 0.77, and 0.53 is shown respective to the listed concentrations range. The best line of fit was added and is y = (2.21±0.1)x + (0.38±0.8) with R^2 = 0.9928.

The optimization of flow rate was performed as illustrated in Figure 8. The peaks represent a reduction of 2.50mM $K_3Fe(CN)_6$ at a different level of flow rates. An assumption was made that a slower flow rate increased the peak area. The area under each peak was verified with the old traditional method of calculation where the mass of each peak (paper) and a 1x1cm^2 were proportionately compared. As a result, the area of the first peak, second peak, and third peak were determined to be 24.86μC, 28.29μC, and 31.71μC (μA*s) at 400, 300, and 200 μL/min flow rate respectively. This confirmed that the peak area was increased as the flow rate decreased, which is proportional to the amount reduced, as expected. Furthermore, it is known that the mass transfer-limited

currents for different cell geometries follow a particular set of equation.[8] The thin layer cell is a wall jet electrode geometry that accounts for ¾ factor of the flow rate as indicated in equation 7

$$i = 0.898nFCD^{2/3}v^{-5/12}a^{-1/2}A^{3/8}\upsilon^{3/4} \tag{7}$$

where a is the diameter of jet inlet, v is the kinematic viscosity, υ is the flow rate, and others are the same. If the limiting currents are known at given flow rate, a plot of i vs $\upsilon^{3/4}$ can be constructed to interchangeably calculate the unknown parameters by using the literature values. Using the literature value of diffusion coefficient of $[Fe(CN)_6]^{3-}$ can determine the kinematic viscosity and using the literature value of dynamic viscosity of $[Fe(CN)_6]^{3-}$ can determine the kinematic viscosity ($v = \eta/\rho$) and therefore determines the diffusion coefficient.
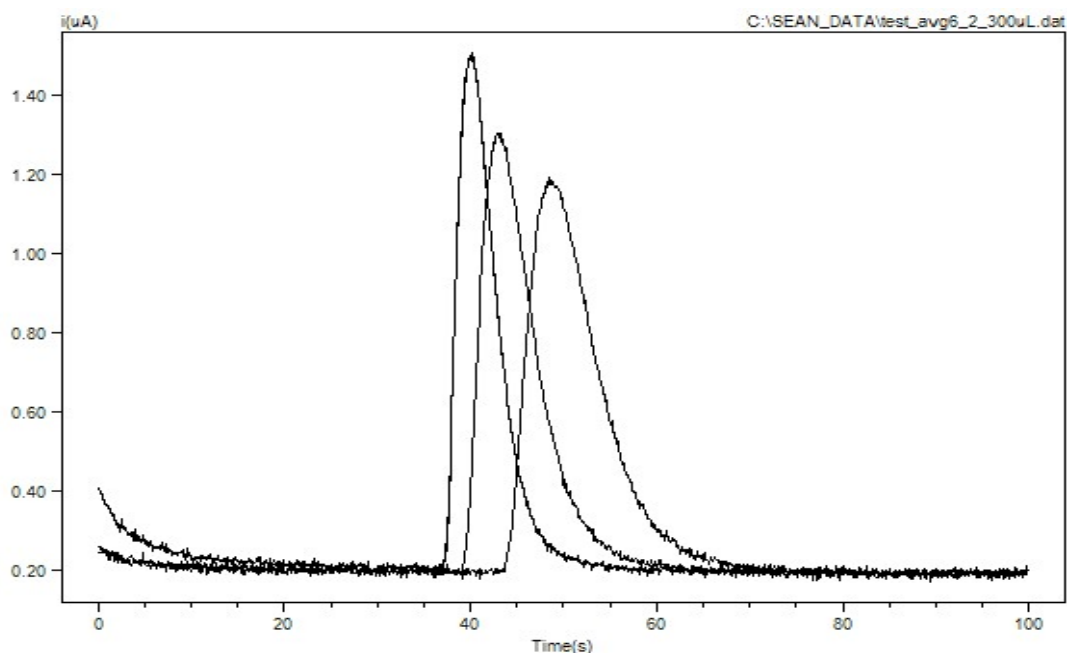
Figure 8. A comparison of reduction peaks of 2.50mM $K_3Fe(CN)_6$ injected into the thin-layer cell at different flow rates. The flow rate was, from the left peak to right, 400uL/m, 300uL/m, and 200uL/m, respectively with other CA conditions held constant: initial E(V) = -0.3V, High E(V) = -0.2V, Low E(V) = 0.3V. Pulse width(s) = 100, sample interval(s) = 0.1, Quiet Time(s) = 10, Sensitivity(A/V) = 1e^{-5}.

Figure 9 further analyzed the effects of flow rate respect to current-time profile (i vs t). At a flow rate zero, the quiet charge is found to be 38.56µC by plugging in 0 for x at the trend line created in Figure 8. The negative slope regression showed that the increase in flow rate caused smaller peak intensities, shorter reaction time on the surface electrode, and therefore lesser moles of samples are reduced. Furthermore, the detection limit was calculated from the error in the intercept. Using a signal-to-noise ratio of 3, the error was multiplied by 3 and equaled 0.027µC. The background noise was determined to be 0.2µA or 0.025mM and using a simple equation, it=Q where Q is the intercept from the calibration curve, the time of the baseline was calculated as 193seconds. Dividing the

error, 0.027μC by 193seconds gave a value of 1.4E-4μA, or 0.14nA (17.5nM), equivalent
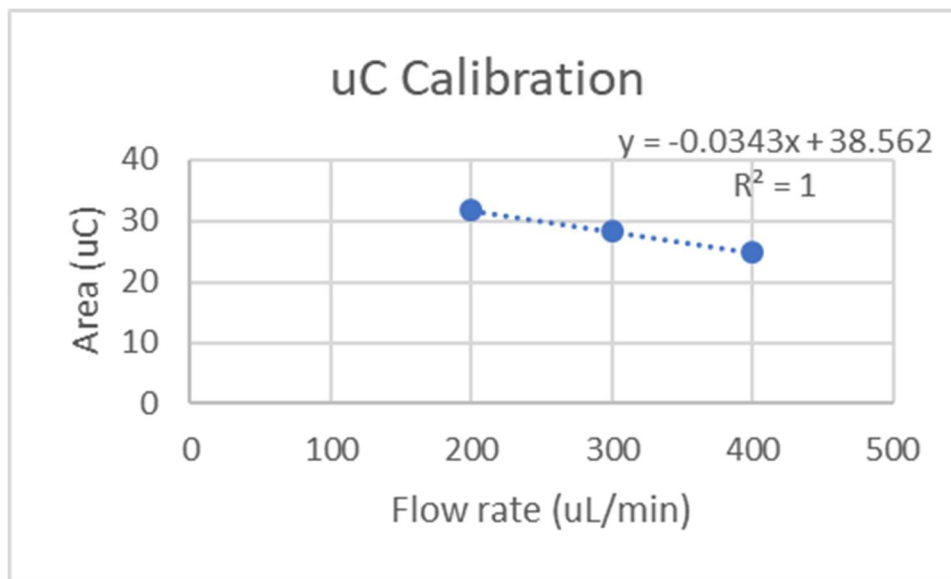
to the detection limit.

Figure 9. A Calibration curve of the area obtained from Figure 8 by the corresponding
flow rates. The best linear fit data gave a slope of -0.0343±0.00003 with the y-intercept
of 38.562±0.009, which is the base line when x (flow rate) equals 0, with R2 value of 1.

Anodic stripping voltammetry (ASV) was performed to further analyze the trace

metal ions in aqueous samples. ASV is usually for the measurement of trace

concentrations of metal ions in samples, but this experiment was performed to examine

the degree of reversibility of the thin-layer cell. The electrochemical potential window

from -0.8mV to +0.1mV was selected to prevent the oxidation of Hg and the removal of

Hg from the Hg-layer. Figure 10 shows the ASV of three metal ions with peak potential

close to the standard reduction potential of the metal ions. Peak currents are diffusion

controlled if the deposition potential is set far negative of the standard redox potential vs.

SSC reference. The very first peak at potential -0.2V corresponds to Cu/Cu^{2+}, -0.5V corresponds to Pb/Pb^{2+}, and -.65V corresponds to Cd/Cd^{2+} metal ion.
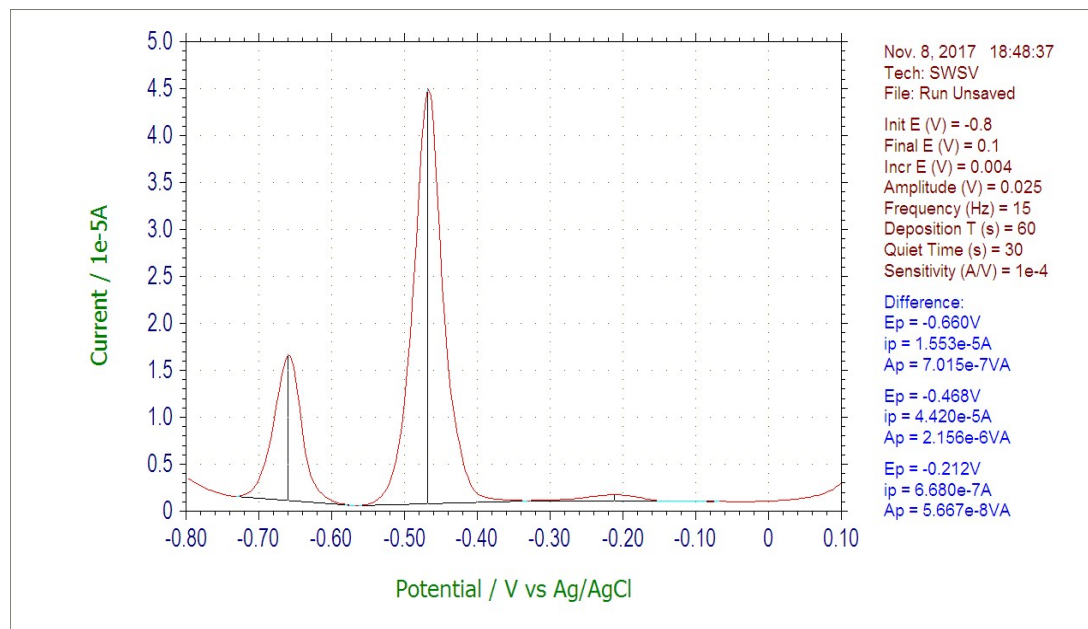

Figure 10. Anodic stripping voltammetry of 100ppm Cd^{2+}, Pb^{2+}, and Hg^{2+}. The conditions are as displayed. Reduction peak at-0.66V is Cd^{2+} with ip of 1.553E-5A, Pb^{2+} had Ep at -0.468V and ip of 4.420E-5A. The third is presumably Cu with -0.212V and 6.680E-7A.

Equation 3 ($W_{1/2} = 3.52RT/nF$) was employed in the stripping voltammogram to determine the degree of reversibility of the electrochemical reaction which is proportional to the number of electrons involved in the reaction. The part, 3.52RT/F can be treated as a constant number 90.4mV and a division by the half width potential determines the variable n.[8] The half peak width was measured by looking at half of i_p value and subtracting both end of the parabola. The calculated n value for Cd^{2+} and Pb^{2+} were approximately 1.8. The difference in actual n value of the metal ions were very minimal,

30

but the numbers of electrons involved in the reaction of both were the same; oxidation

number of 2+ charge, equally gaining $2e^-$ in the half-cell reaction.

These experiments were performed before venturing into a much smaller flow cell

volume in the microfluidic channel to better understand the flow system and its efficiency

based on optimal conditions. This easily fabricated flow cell verified its capability and

potential that can be further extended and improved upon using much smaller and

versatile microfluidic channel.

5.2 Electrochemical potential modulated microchannel (EPMM) device

After optimizing the first flow cell with $[Fe(III)(CN)_6]^{3-}$ and observing its

potential in critically evaluating the trace metals, a microfluidic channel (a gift from

Professor Yoon Bo Shim[2]), was examined. The most important characteristics of this

device are the integration of a separation channel and an electrochemical detector in one

piece. The channel was fabricated by using the microlithographic technology used in the

electronics industry. It consists of glass microslides with multiple layers of carbon ink

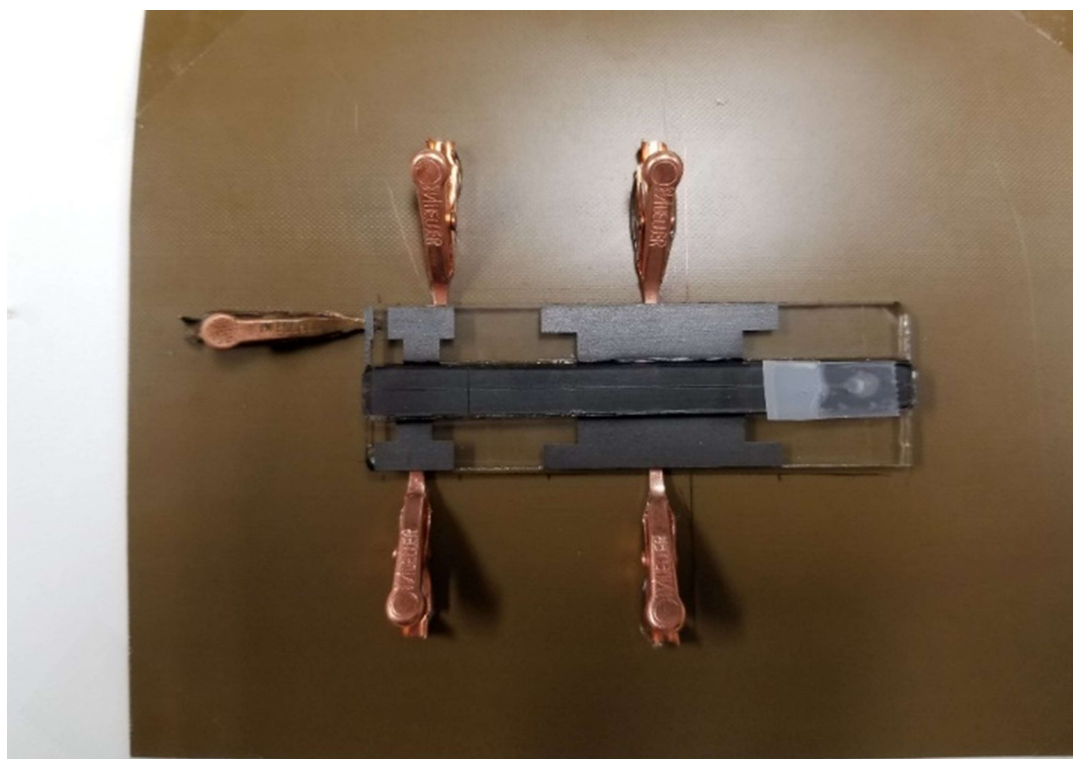onto the slides as shown in Figure 11.

Figure 11. A Photograph of the microfluidic channel device. The injection port is on the right side (taped to prevent dust accumulation). The total channel length is 67.0mm, the width of the separation channel is 95.0±2.5µm, and the width of the detection channel is 90.0±1.5µm. The separation channel itself is 52.0mm long, working electrode (bottom left) is 15.0mm, counter electrode (upper second to left) is 12.7mm, and reference electrode (upper left) is 2.0mm.[2]

The experimental apparatus was similar to that of the first flow cell but the application of alternating current (AC) potentials in the separation channel. The AC potential was generated and applied to the channel walls using a waveform generator/oscillator, which is illustrated later. This different setting of AC electric potential to the EPMM device brought multiple effects on electrode properties as well as solutions themselves influencing the separation of redox species before electrochemical detection as claimed by the authors.

Some of the preliminary experiments with the EPMM device were characterization of the detection electrode using supporting electrolyte such as determining the double layer properties, baselines, and charging currents. Then, the AC electric potentials using a waveform generator was applied affecting the redox properties of the analyte $[Fe(III)(CN)_6]^{3-}$. The same experiment was performed with different AC frequencies. A general scheme of the experimental set up is shown in Figure 12.
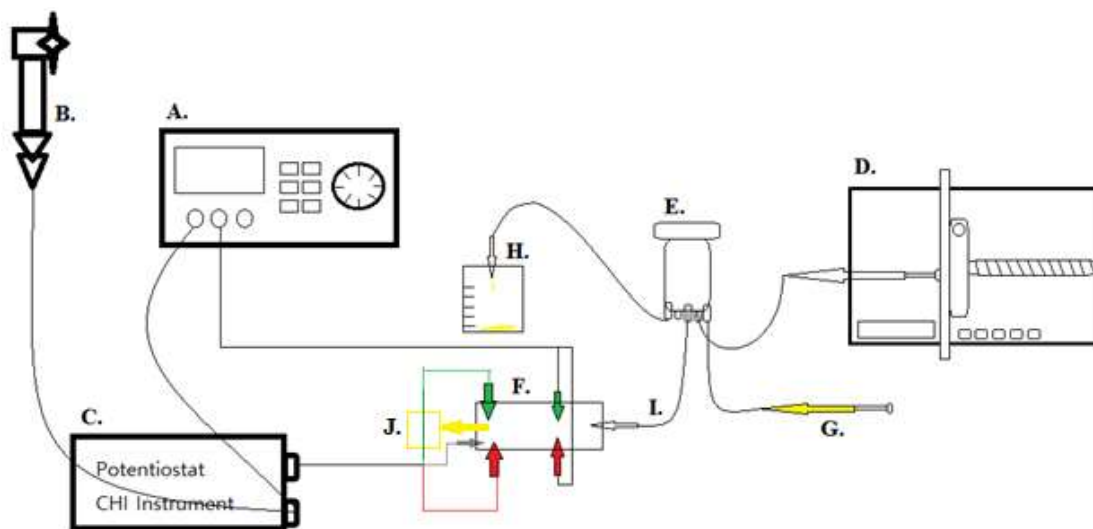
Figure 12. General scheme of the apparatus. **A**. waveform generator, **C**. potentiostat, **F**. EPMM device with three alligator clips to the three electrodes of the electrochemical detector, **E**. 6-way injection port, **D.** automated syringe pump, **G.** analyte syringe, **H.** waste syringe/container, **I.** injection syringe, **B.** metal faucet (as electrical grounding), and **J.** waste collecting filter paper.

5.2.1 Preliminary experiments

The primary experiment with the supporting electrolyte was to determine the baseline and charging current vs. SSC and further demonstrate dielectrophoretic

phenomena, which describes the interaction of electric fields with dielectric (electrically neutral) particles like water.[13] On the first experimental trial to initialize the background, the responses from the devices were experiencing heavy noise levels. Thus, establishment of the common ground for devices was necessary before any further experiment. Two pieces of alligator clips were used to ground the potentiostat and the waveform generator to reduce the noise that electronics typically generate as shown in Figure 12. Both devices were grounded to a metal faucet as the internal conductor for common ground (0V) reference potential for electronics. As a result, the grounding was successful as the noise was noticeably reduced as shown in Figure 13. In order to show the reduced noise, the grounding was established at 65seconds.
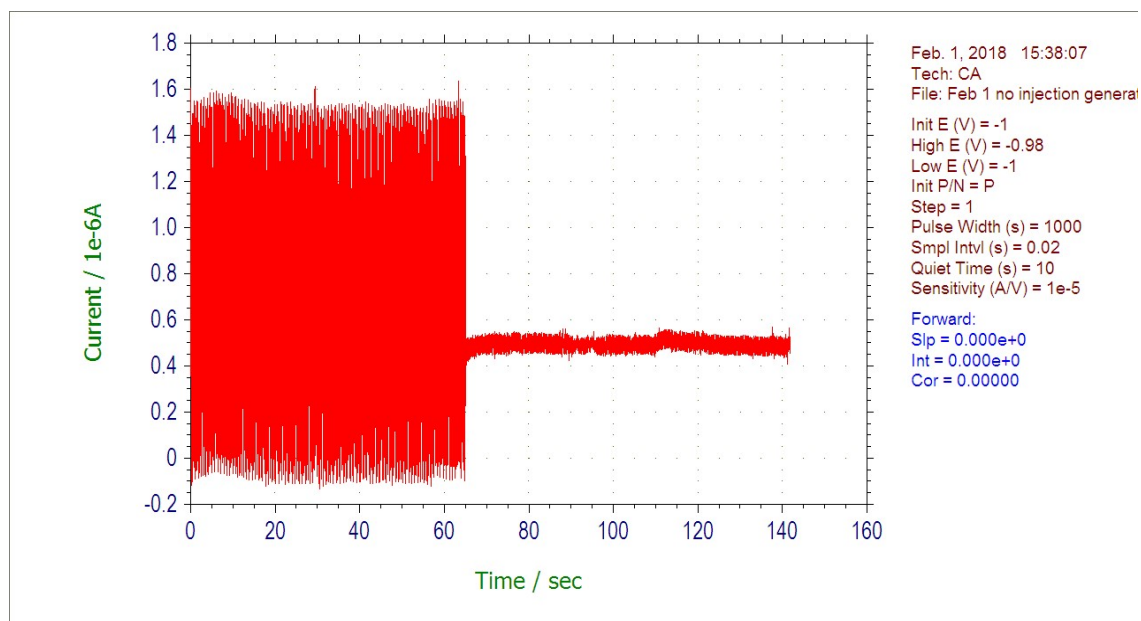

Figure 13. Chronoamperometric response of the microfluidic device with supporting electrolyte. Grounding test of the supporting electrolyte. No grounding before 65seconds. After 65 seconds, extra metal clips were attached to one, metal faucet to potentiostat and two, potentiostat to waveform generator as illustrated in Figure 12.

Additional background voltammograms were recorded to measure the electrochemical window. The purpose was to obtain the effective electrochemical window of the electrochemical cell on the EPMM device and establish the baseline voltammograms. A CV scan of acetate buffer and the response exhibited by the electrochemical detector determined the effective electrochemical window as shown in Figure 14. The scan started at 0 and cycled through -1.5V to +1.1V vs. SSC three times.
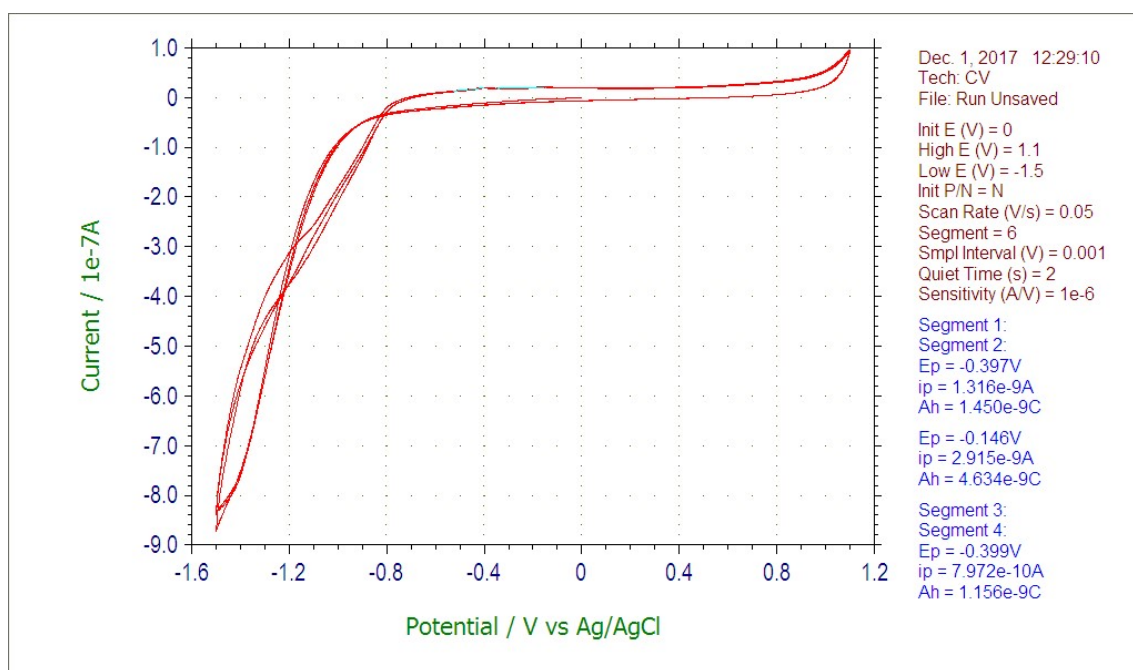
Figure 14. CV scan of acetate buffer flowing through the microfluidic channel and detected by the electrochemical detector. The scan starts at 0 and cycled through -1.5 to +1.1 V vs. SSC three times. The increase in oxidation current shows the evolution of hydrogen from water. The effective electrochemical window is +-1.0V vs. SSC.

Due to an increase in oxidation current at the negative potential region, it was clear that the evolution of hydrogen from water was occurring. Also, another increase in

oxidation current occurred at potential greater than 1.0V which was an indication of oxidation of water to O_2 evolution. However, an extended scan of the positive potential region 0 to +1.0V vs. SSC was recorded due to a relatively smaller gradient. Although the hydrogen evolution due to reduction of H^+ was indeed bigger and faster near -0.8V, the oxygen evolution was not noticeable at +1.1V as shown in Figure 15. This concluded that ±1.0V vs. SSC was the effective electrochemical window within which redox species can be measured.
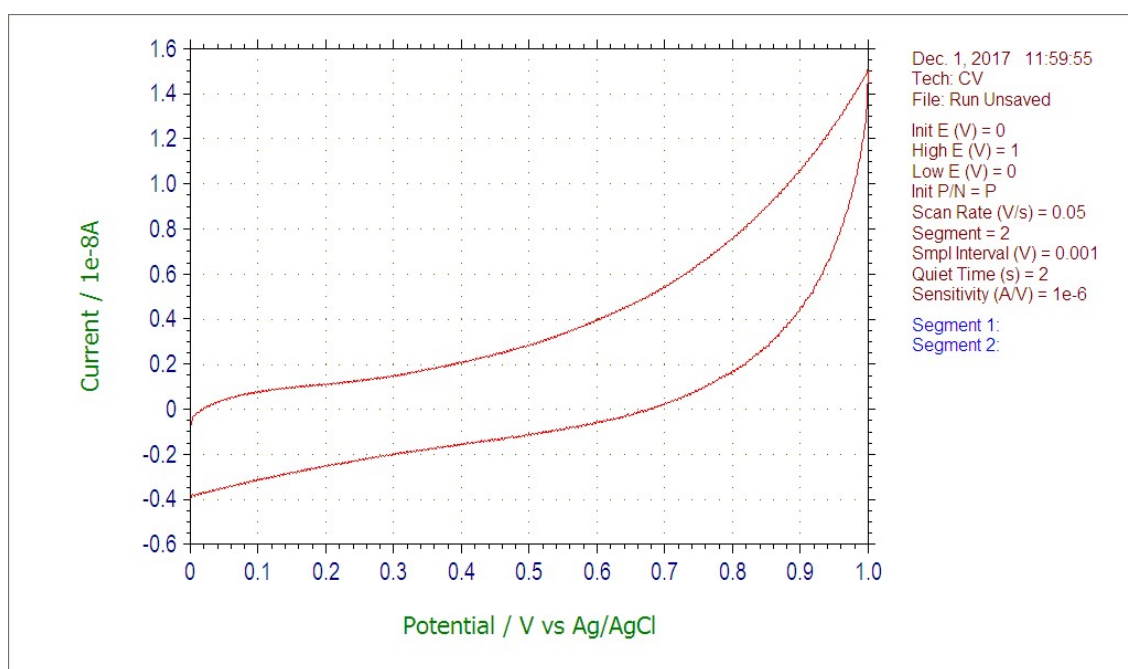
Figure 15. An expansion of CV scan from Figure 14 in the positive potential region, from 0 to +1V, showing some oxidation of water to oxygen evolution from an acetate buffer solution. Compared to hydrogen evolution the oxygen evolution is much less and kinetically slower on the carbon electrode.

Further analyses to find the baseline, charging current, and double layer properties were performed using the system. The compiled datum from double pulse

chronoamperometry and chronocoulometry scans contributed in determining the electrochemical properties.

5.2.2 Measurement of double-layer properties of electrochemical cell on the EPMM device

A non-Faradaic process can be demonstrated and then characterize electrochemical cell properties by the chronocoulometric technique. Also, since the major goal is to observe the effects of applied AC potential, two responses with and without the AC potential were compared. A double pulse chronocoulometry of an acetate buffer without AC potential is illustrated in Figure 16.
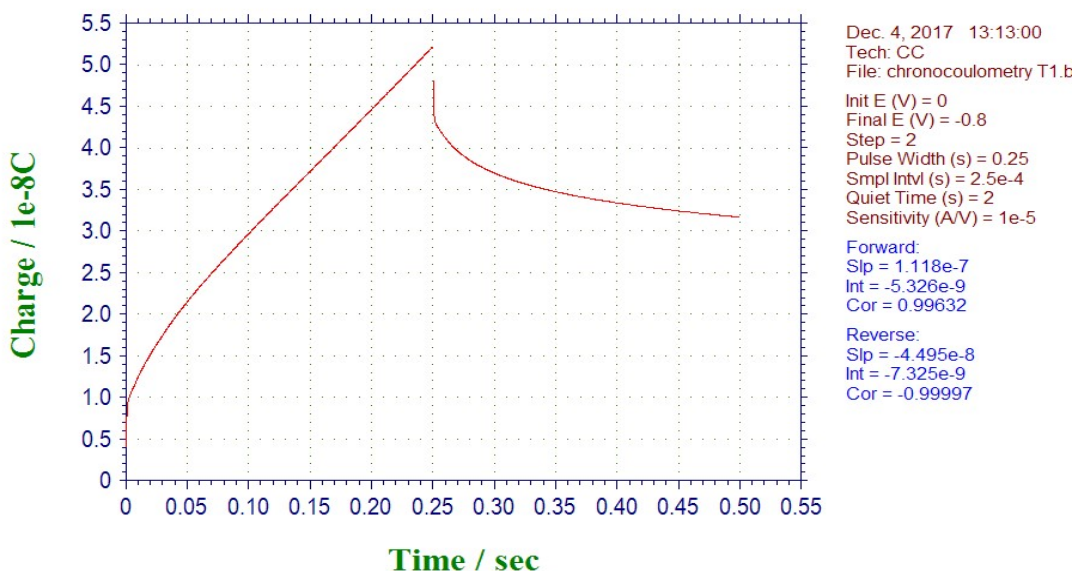

Figure 16. Double pulse chronocoulometry of an acetate buffer to calculate the double layer properties of the electrode from slopes and intercepts of the forward and reverse pulse. The potential pulse is set from 0 to -0.8V, pulse width of 0.25s, sample intervals of 2.5e-4, quiet time of 2s, and sensitivity of 1e-5A/V.

Evidently, Anson popularized and employed CC in place of CA because it offered experimental advantages: CC offers better signal-to-noise ratio and therefore least distorted transient, CC has a smooth random noise integration on the current transients, and CC can be used to distinguish the adsorbed species from the double layer properties.[8] However, Anson's and Cottrell's models are only applied for Faradaic processes on electrodes. Therefore, a derivation to these models was performed to determine the double layer properties of the system. The integrated form of equation 5 ($\ln[i(t)] = \ln(E/R_s) - t/\tau$) is given by

$$Q = E\,C_d\,e^{-t/\tau} \tag{8}$$

where E is the charge, C_d is the double layer capacitance, and τ is the time constant. These parameters will be determined while going over the effect of AC potential (CC technique) for comparison purposes.

The responses with and without AC potential on the EPMM device were recorded and quantitatively analyzed. The time constant and double layer capacitance of the electrode were calculated for both with and without AC potential and compared. The experiment confirmed the effects of AC potential induced field on non-Faradaic process. An illustration of overlaid CC plot of with and without AC potential is shown in Figure 17.
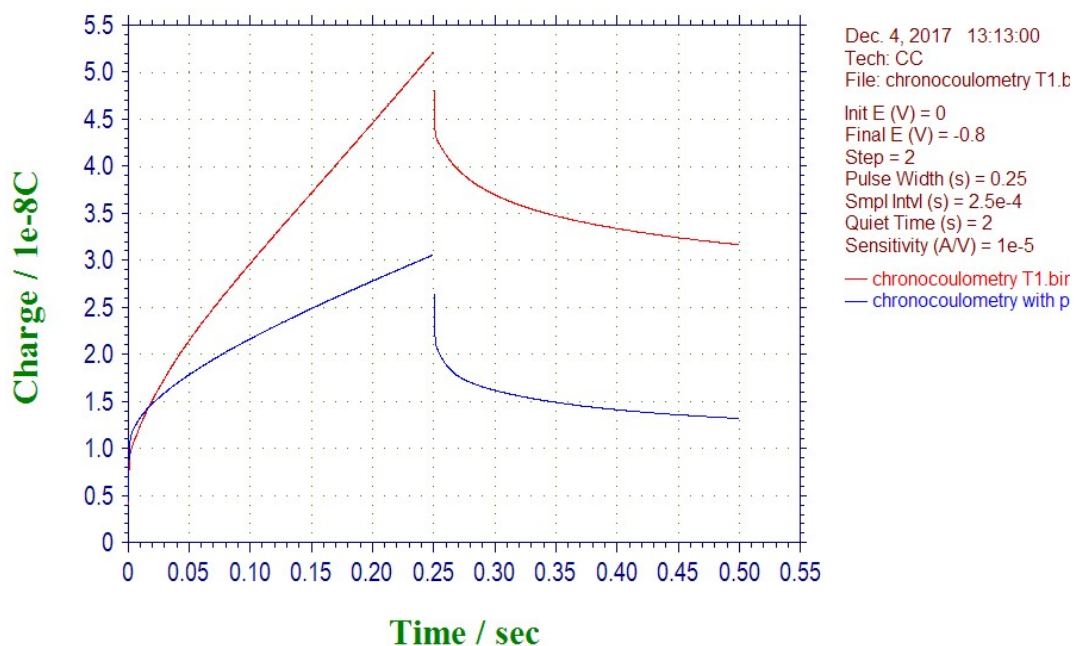
Dec. 4, 2017 13:13:00
Tech: CC
File: chronocoulometry T1.b

Init E (V) = 0
Final E (V) = -0.8
Step = 2
Pulse Width (s) = 0.25
Smpl Intvl (s) = 2.5e-4
Quiet Time (s) = 2
Sensitivity (A/V) = 1e-5

— chronocoulometry T1.bir
— chronocoulometry with p

Figure 17. Double pulse chronocoulometry of an acetate buffer with and without application of AC potential. The red indicated without and blue is with AC potential applied. The pulse potentials and other conditions are kept the same for both experiments as indicated in the figure.

The application of AC potential had an impact on the response as shown in Figure 16. The peak intensity as well as the slope in the forward reaction were halved when total amplitude of 1.0V AC potential was applied to the channel wall electrodes. The AC potential reduced the residual analyte half the time and reducing the concentration of the analyte in half as shown by the reduction of charge in the electrochemical detector. This is also known as AC electrolysis. While only an acetate buffer was being analyzed, applying AC potential had reduced the charge passed indicating the presence of residual electroactive species. More specifically, a residual electroactive species was present and influenced the forward, or reduction reaction, response.

Along with the acetate buffer, there is a very small amount of dissolved oxygen (O_2) present as a residual electroactive species. When an AC potential of $\pm 0.5V$ is applied to the carbon channel walls, O_2 reduction to hydrogen peroxide (H_2O_2) occurs at the negative potential interface, where standard reduction potential vs SSC is 0.475V.[8] Because O_2 is not reversible, applying a positive AC potential does not oxidize H_2O_2 back to O_2 leaving all the reduced H_2O_2 undetected at a given potential pulse. As a result, the reduced amount of oxygen was detected at the electrode shown by smaller peak intensities. A further comparison of the electrode/solution properties affected by AC potential was reported from the plot, ln(Q) vs time, shown in Figure 18.

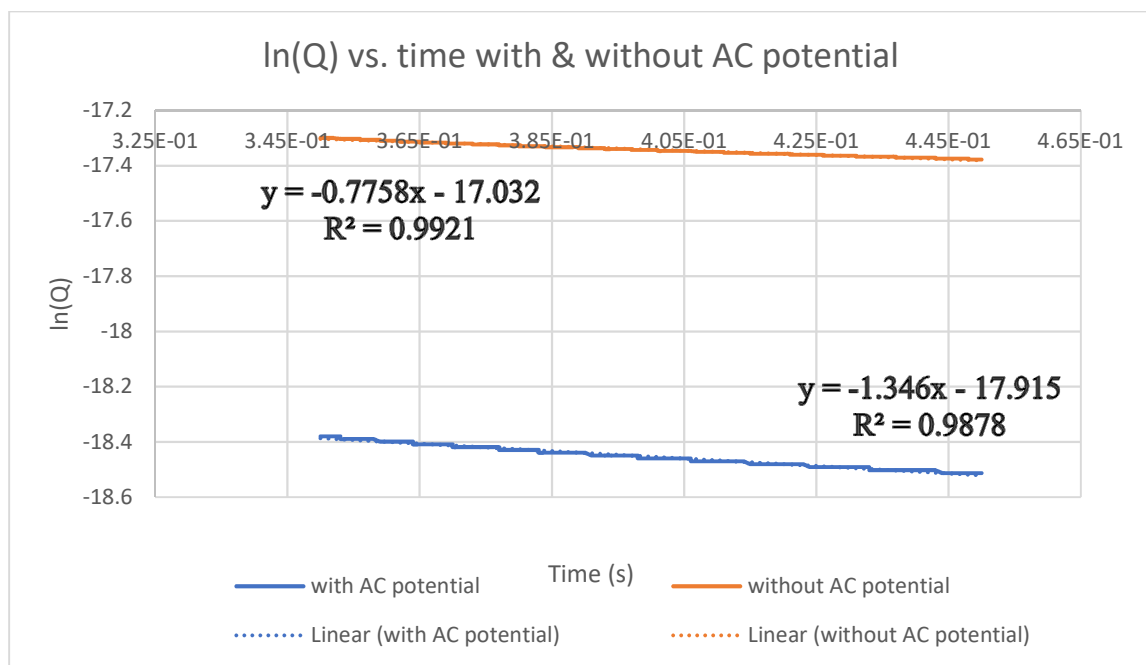**Figure 18**. A plot of two forward pulses and linear regressions of ln(Q) vs. time (s) from the most linear lines of the second step pulse, background subtracted. Both reaction time starts from 0.35 to 0.45 seconds. The trend line with AC potential (blue) is y = (-1.346$\pm$0.007)x – (17.915$\pm$0.003) with $R^2 = 0.988$. The trend line without AC potential (orange) is y = (-0.776$\pm$0.003)x – (17.032$\pm$0.001) with $R^2 = 0.992$.

The linear portions of the CC responses were analyzed to calculate the double-layer properties C_d and τ. By plotting the log of charge vs time of equation 9, one can calculate the time constant, τ, and the double layer capacitance, C_d of both experiments shown in Figure 18.

$$\ln(Q) = \ln(EC_d) - t/\tau \tag{9}$$

Given that the slope equals to $-1/\tau$, the time constants were calculated: τ with AC potential was 0.743 ± 0.007 seconds and τ without AC potential was 1.289 ± 0.003 seconds. The smaller τ with AC was probably due to a cleaner solution with less redox impurities in solution.

As previously mentioned, because IPE, ideally, behaves similarly to RC charging circuits, the electrode system built here suffers from some form of time delay between its input and output called time constant. The time constant is measured in τ is a measure of the response time when a step potential is applied to the system. From the calculated value above, it was clear that the application of AC potential not only reduced the amount detected, but also reduced the rate of charging and discharging of the double-layer. This suggested that applying AC potential to the separation channel (not the detection cell) facilitated the charging current process of the detection cell. This is further explained by Figure 19.
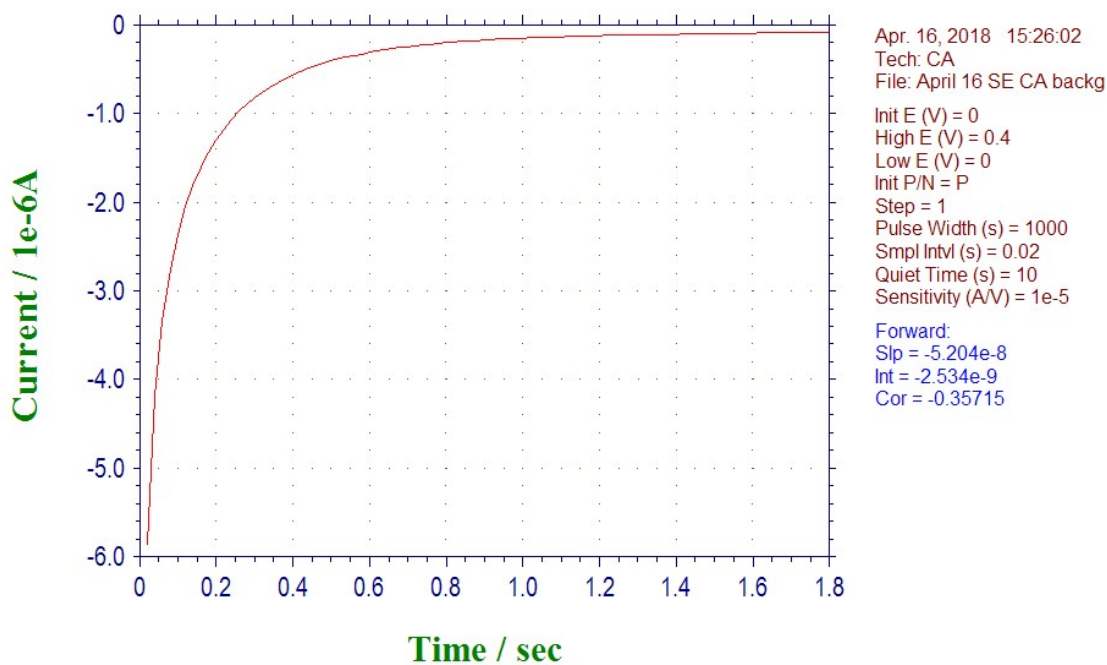
Figure 19. An expanded chronoamperometric record of the supporting electrolyte at potential from 0 to 400 mV vs. SSC. No AC potential is applied in the separation channel.

The purpose of looking into the charging current is because of its significance in measuring the total current, especially for low faradaic currents as well as in IPE system where the charging component of the current determines the detection limit of the technique. The values of charging current shown in Figure 19 and the time constant from Figure 18 (without AC potential) are comparably similar. Figure 19 shows the steady state current is about -0.15μA.

Since the y-intercept from Figure 18 is directly relevant to the value of double layer capacitance, resistance and other properties of the system were calculated by simple algebraic rearrangements. Using the relationship of time constant (R_s x C_d), C_d was

calculated to be 50.12±0.05 nF. Thereafter, the resistance of the supporting electrolyte

was (2.57±0.03) x $10^7\Omega$. The same calculations were performed under the affect of AC

potential. However, the magnitude of the numbers was not so different from the previous

experiment (without AC potential) because of the unchanged electrode-solution interface.

This is expected because, the separation channels are completely isolated from the

detection electrode. The values were 20.73±0.06 nF and (3.58±0.09) x $10^7\Omega$. A slight

decrease in the capacitance, but an increase value of resistance of the solution between

the conductors was observed. This result is, once again, explained due to residual

electroactive species as mentioned above with the CC experiment; the accumulated

charge of the reduced amount of electrolyte is stored less and therefore the resistance

increases.

5.2.3 AC excitation potential on the redox behavior of ferricyanide in the EPMM device

Redox couples can also be examined by a double potential step CA given its

reduction and oxidation characteristics, the two excitation steps. The responses and the

potential steps are carefully chosen so the reaction is completely diffusion controlled and

there is no electron transfer unlike CV where electron-transfer reaction is a key factor.

The currents resulting from reduction and oxidation (cathodic and anodic) are measured

by the diffusion-controlled region with respect to time.

To examine the effect of channel AC excitation potentials on the redox behavior

of $[Fe(III)(CN)_6]^{3-}$ signal, two experiments were conducted with the same

electrochemical conditions but applied AC potentials. The electrochemical conditions of

initial and final potentials were determined by the CV scans conducted prior to this experiment. The system exhibited a diffusion control current for $[Fe(III)(CN)_6]^{3-}$ at around -0.48V. After the injection of $[Fe(III)(CN)_6]^{3-}$ at a flow rate of 4µL/min resulted in a reduction peak at around 200 seconds. This was due to travel time of analyte from the 6-port injection valve tube through the microfluidic channel and into the detector part of the channel. Two peaks were overlaid in which the peak in red represents the response without the AC excitation potential and the blue represents the response with the applied AC excitation potential as shown in Figure 20.
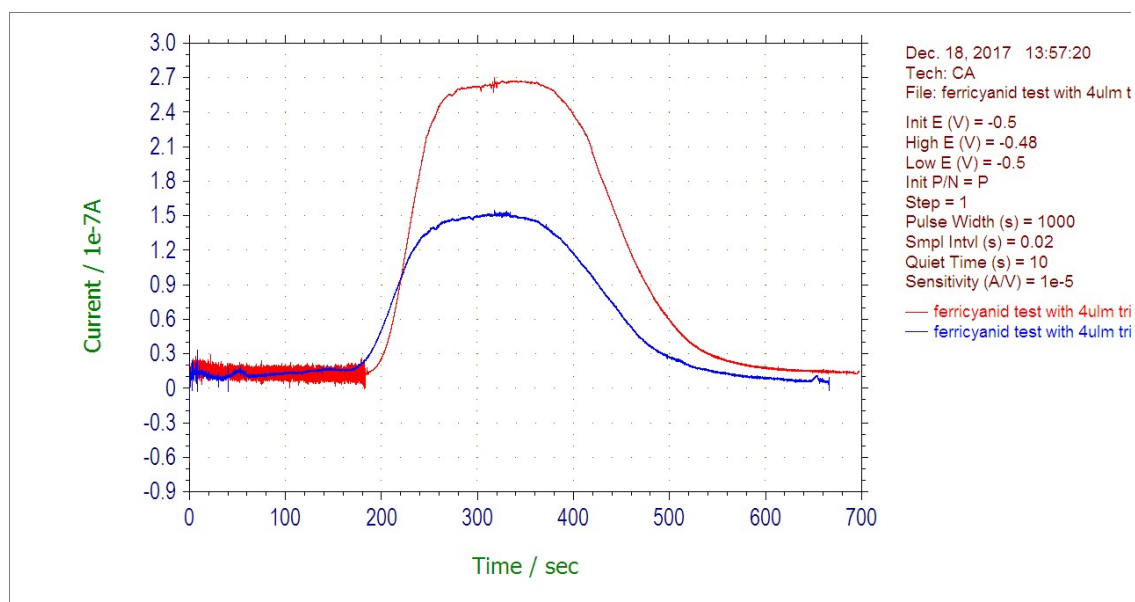

Figure 20. Effects of channel AC excitation potential on the redox behavior of $[Fe(III)(CN)_6]^{3-}$ signal. The curves are under the same condition except the red is without AC potential applied and the blue is with a 0 - 1.00 V, 1 MHz AC potential applied. Electrochemical conditions are shown in the figure.

The illustration clearly shows different intensities of the peaks due to applied AC potential. Applying a square wave potential from 0 to 1V at 1MHz frequency reduced the peak intensity by half, directly correlating to the amount reduced. This AC electrolysis phenomena happens when $[Fe(CN)_6]^{3-}$ is reduced to $[Fe(CN)_6]^{4-}$ ions. When the step potential of 1V is applied to the channel, the reduced $[Fe(CN)_6]^{4-}$ is on the wall half of the time while flowing. This results in half of the $[Fe(CN)_6]^{3-}$ amount reduced detected. This experiment clearly demonstrated that electroactive species can be oxidized and reduced in the channel by the AC applied to the excitation electrodes.

This experiment was also used to measure the volume of the fluid channel. Although the dimensions of the EPMM channel were given in the journal, more accurate measurement of the volume of the fluid channel was calculated from the above signal. This EPMM device used was more of a prototype and therefore the volume had a slight change. Considering two flow tubes, with a sample injection loop volume of 4.94μL and the flow tube volume of 7.60μL. The time of the first response peak started around 189second. Given that the flow rate was 4μL/m, the first detection was shown after delivering 12.6μL (189s/60s*4μL/min). Subtracting the volume of the tubes left a volume of the channel to be 0.0660μL or 66.0nL. Comparison with the theoretical volume from the dimension stated above, a percent error of 11% was calculated. This, however, could have been accounted as a nonideal channel as it is a prototype EPMM. Another source of error could be from not knowing the exact time frame of first response because the data was collected every 0.02second.

5.2.4 The effect of frequencies on the redox behavior of ferricyanide in the EPMM device

After completing the AC excitation potential on the redox behavior of ferricyanide in the EPMM device and verifying the affect, similar experiments with varying frequencies were performed. Frequency dependencies on the redox current changes were observed at 1Hz, 1kHz, 100kHz, 500kHz, and 1MHz with 1.0V peak-to-peak excitation as illustrated in Figure 21. The trend in signals were determined to have a slightly decreasing peak current when AC frequency increased. This experimental result can be explained by Hayden's works where tests on AC electrolysis on multiple electrolytes were performed.[10] Hayden's work concluded that AC electrolysis reaction rate decreases with frequency and that higher frequency decreases the reaction rate. Not only is this observation proven by Hayden, but also the modern theoretical works on electrochemical analysis have claimed that high frequency influences the potential drop on electrical double layer and thus decreases the reaction rate.[10]
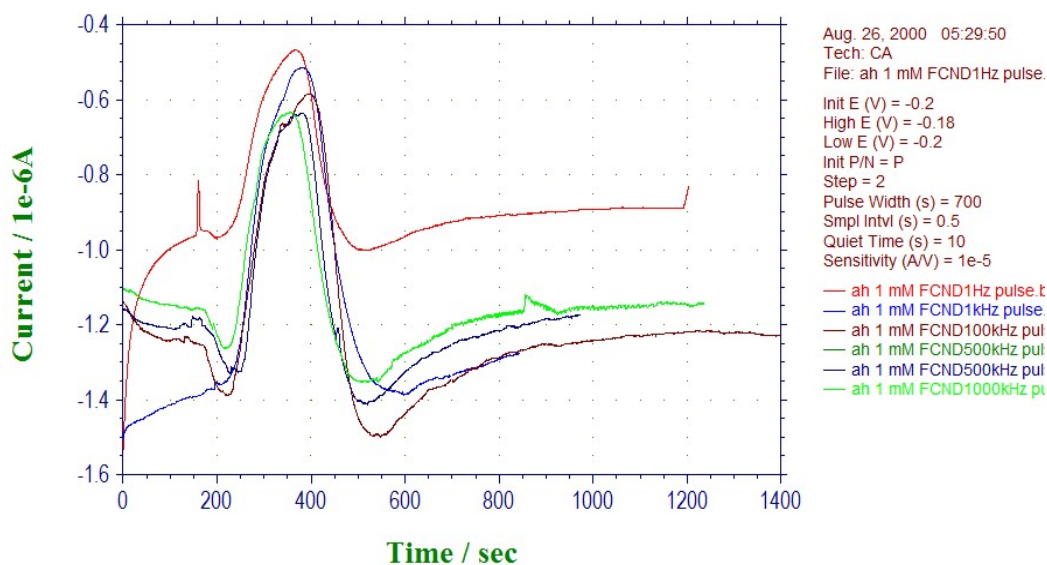
Figure 21. Effects of different AC frequency on the redox behavior of $[Fe(III)(CN)_6]^{3-}$ signal. The curves are under the same condition except varying frequency levels of 1Hz, 1kHz, 100kHz, 500kHz, and 1MHz. The electrochemical conditions of chronoamperometry are as shown in the figure.

Evidently, the current drop resulting from an increase in AC frequency matches the previously mentioned works. As inferred earlier, Faradaic reaction reducing ferricyanide becomes quantitatively limited, thus slowing the reaction of producing or decreasing the amount of detected ferrocyanide. Relating this experiment to AC excitation potential, both follow the same trend where applying AC potential and frequency reduces the moles of ferrocyanide detected. The observed effect is significant at 1Hz. Frequencies higher than 1KHz, the effect is not drastic to an extent that the technique is analytically impaired. However, the most important effect of AC modulation on the separation of chemical species in the channel was not examined in the work.

5.2.5 Cleaning the EPMM device using chronoamperometry.

After the characterization experiment with $[Fe(III)(CN)_6]^{3-}$, a CA run of cleaning

was performed to clean out the electrode. Figure 22 confirmed that the reduced

$[Fe(II)(CN)_6]^{4-}$ was not oxidizing back to $[Fe(III)(CN)_6]^{3-}$ compound at the cleaning

potential. After experiments, metal ions cleaning involved only the flow of supporting

electrolyte to observe any of the remaining metals on the electrode surface. Since all

metal ions are reduced and deposited at negative potential, positive potentials +1.0V vs.

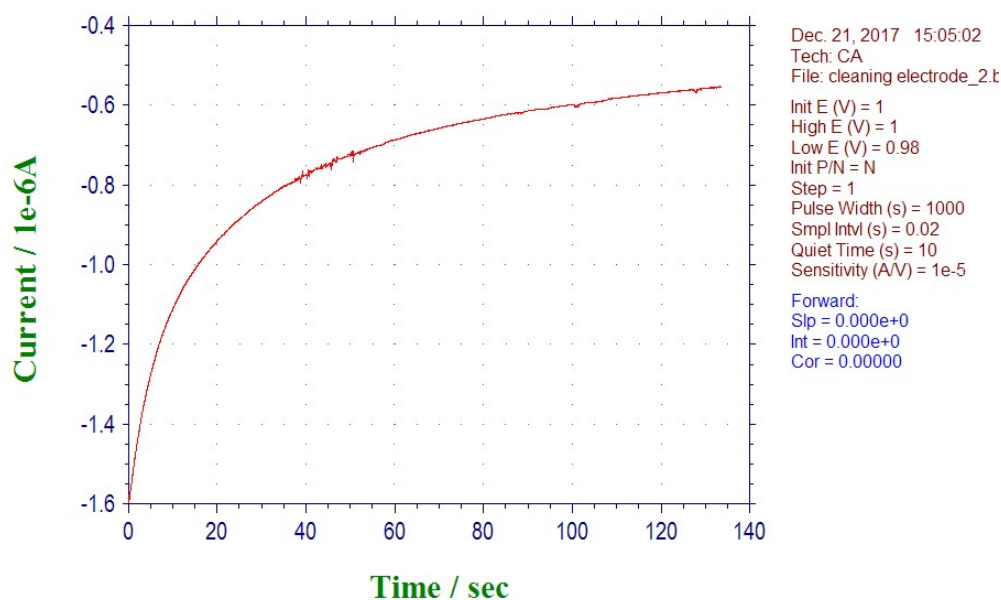SSC was used to clean the electrode.

Figure 22. Cleaning step of the EPMM device with 2.5mM $[Fe(III)(CN)_6]^{3-}$ by chronoamperometry method at positive potential from 0.98V to 1.0V with applied AC potential of 1V.

5.2.6 Measurement of open circuit potential (OCP).

The open circuit potential (OCP) is a measure of the stability of the electrochemical detection cell. The OCP was performed before every run to ensure integrity of the cell. Generally, the OCP is measured with working and reference electrodes when the counter electrode is shorted to the reference electrode, in which no current flows. The result in Figure 23 shows the OCP became stable at 1.0V from the initial potential of 0.8V. A small voltage drop from the initial potential and a noise free transient shows the electrochemical detector is stable and the electrodes are intact with a supporting electrolyte inside the very small 66nL cell.
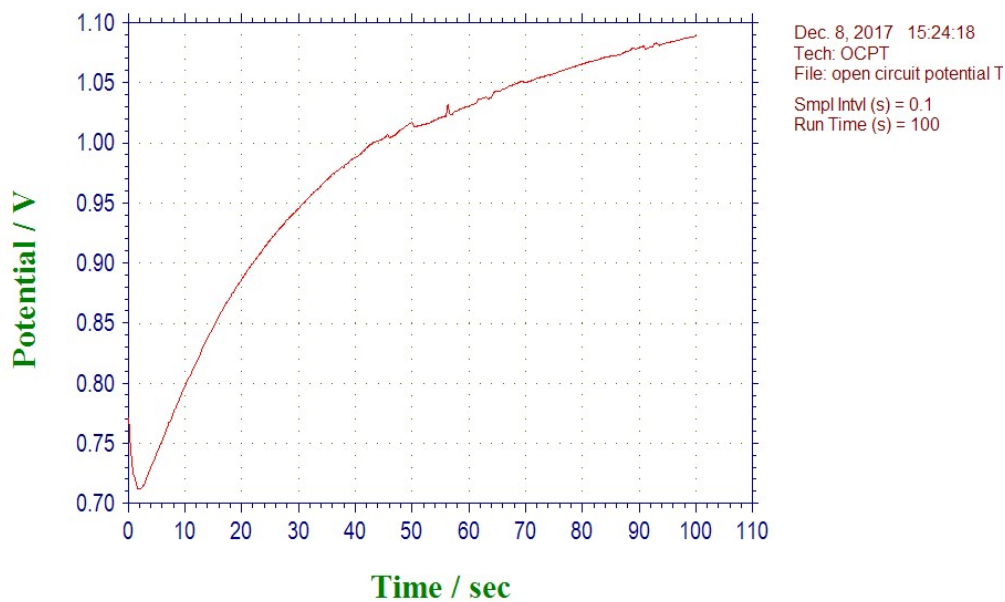

Figure 23. Open circuit potential vs. time (s). Initial potential from 0 to 1.0V and scan rate at 50mV/s. Run time is 100s with sample interval of 0.1s.

5.2.7 Detection of metal with the EPMM device

After the characterization of the EPMM device, a solution containing
combinations of trace metal ions (100ppb each Co, Cd, Cr, Pb, and Se, and 300ppb each
Fe and As) were examined. This sample was prepared by diluting the original stock
reagent prepared from respective nitrate salts in 0.10M HCl with a 4.53 pH acetate buffer
solution. By using the same instrumental set up as described earlier, the metal ions
sample was loaded and injected along with the flowing supporting electrolyte. The AC
potentials were applied to the separation channel. As anticipated, responsive peaks were
detected as shown in Figure 24a, b, c, and d (page 52-53). These are sequential scans
after the sample injection. Due to initial dead-time for the sample to move from the
injection port to the electrochemical detector, the signals were recorded after a 510s
delay. A total of thirteen (13) major peaks with very narrow widths (almost like spikes)
were recorded in Figure 24a, b, c, and d. Two minor peaks were also observed. There are
seven metal ions (Co, Cd, Cr, Pb, Se, Fe, and As) in the solution. Although the peaks
were not identified with the corresponding metal ions, the order of retention should be Cr,
Fe, Cd, Co, Pb, As, and Se according to their standard electrode reduction potential
shown in Table 2. Following the order of retention, the very first reduction peak should
be Cr followed by Fe, Cd, Co, Pb, As, and Se. The extra peaks observed were redox
impurities at trace level. Assuming the peak intensities are proportional to concentrations,
one can find the analytical figure of merits for the technique. Evidently, the second major
peak, presumably Fe, from Figure 24a is one of the highest intensities shown. The
reduced species there, Fe, indeed had the highest concentrations, 5.37μM, among other

trace metals. This concluded that, though metal impurities from the acetate buffer could have caused the unknown peaks, the other peaks shown signifies the detection of metals Cr, Fe, Cd, Co, Pb, As, and Se.

Table 2. Analytical quantification from the detection of metal ions on the EPMM device using chronoamperometry.[8] Reduction potentials (V) vs. SSC was obtained from Bard and Faulkner electrochemistry textbook and sensitivity and detection limit was calculated accordingly.

Metal ion	Cr^{2+}	Fe^{2+}	Cd^{2+}	Co^{2+}	Pb^{2+}	As	Se
Reduction potential (V) vs. SSC	-1.12	-0.66	-0.62	-0.40	-0.35	0.36	0.93
Sensitivity (nA/ppb)	250	83	241	241	184	53	143
Detection limit (ppb)	0.24	0.72	0.25	0.25	0.33	1.14	0.42

The seven major peaks from Figures 24a, b, c, and d were chosen according to their intensities. Cr and Fe from Figure 24a (last two peaks), Cd and Co from 24b (first two peaks), Pb and As from Figure 24c (first and last peaks), and Se from Figure 24d were analyzed. The reduction potentials were obtained from Bard and Faulkner[8] and the sensitivities were calculated from the peak current values. Furthermore, the results including detection limit show that the developed method is sensitive and selective for the detection of these metal ions.
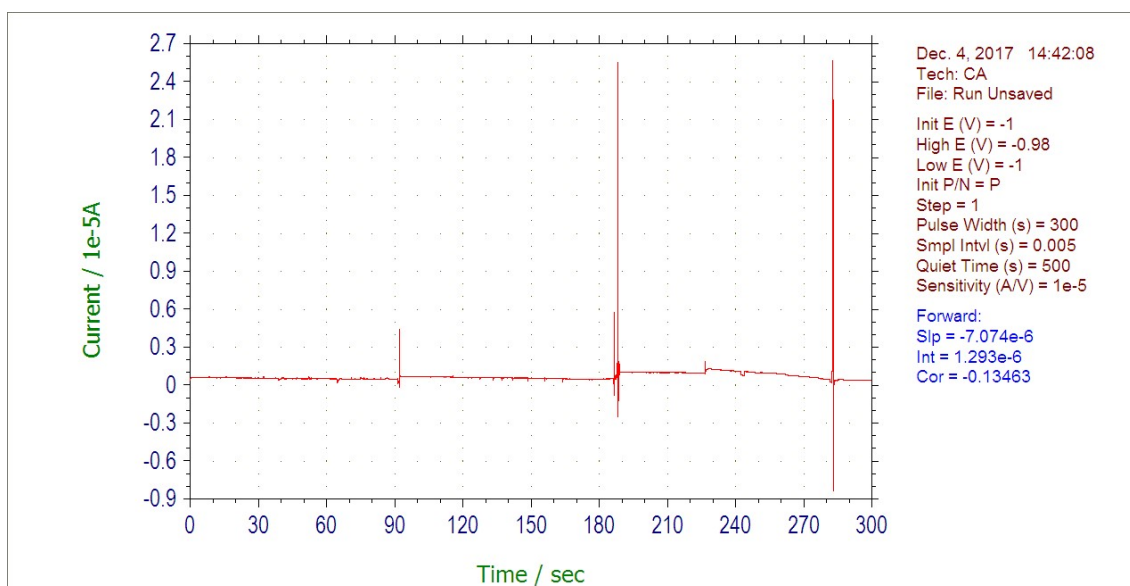
Figure 24a. Chronoamperometric signals of trace metal ions. The quiet time was set to 500seconds after the calculation of optimal wait time until the injection enters the channel. The working electrode potential was set to -1V respect to vs Ag/AgCl. The run time is 300 seconds. Three peaks observed at 90s, 189s, and 284s.
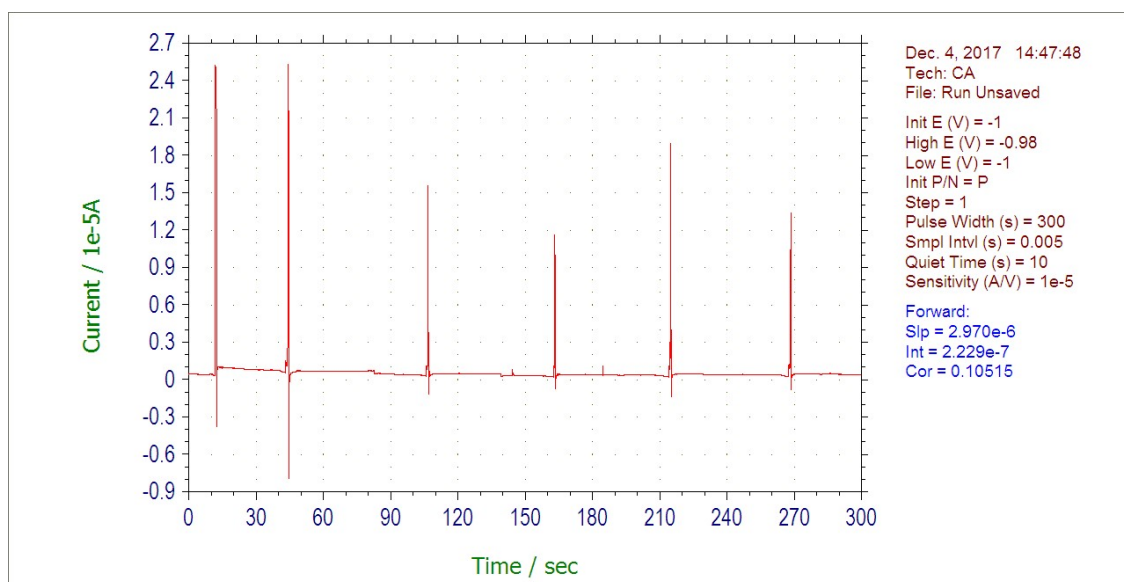

Figure 25b. Continuous same experiment as Figure 23a except there was a shorter quiet time of 10seconds. The purpose was to observe one scan after another for reduction peaks. 12s, 45s, 106s, 162s, 212s, 269s.
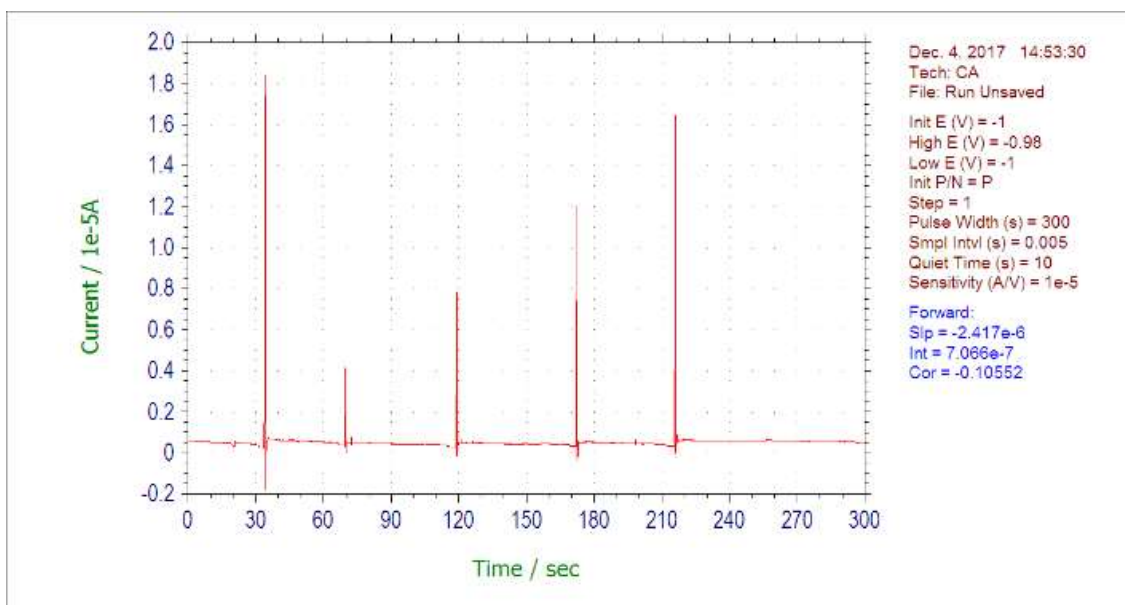
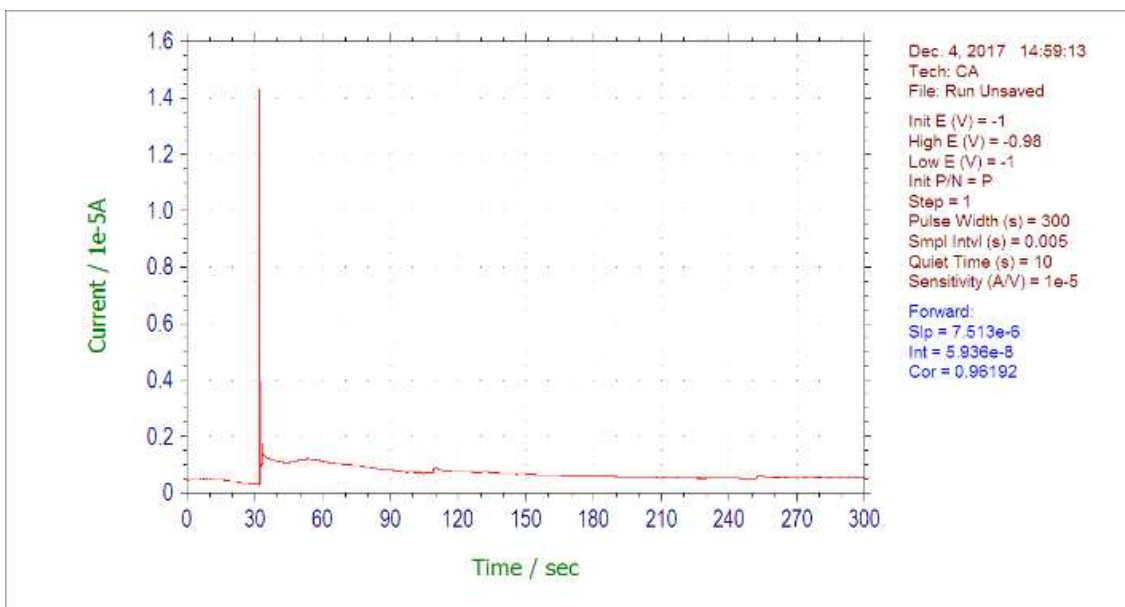**Figure 264c**. Same condition as Figure 23b. Peaks are at 32s, 70s, 120s, 172s, and 213s.

Figure 27. Same condition as Figure 23b. The last peak was at 31s.

6.0 Conclusion and future works

All of the preliminary experiments showed that the experimental setup to work on microfluidic devices was possible. Initial experiments applying different electrochemical techniques showed that the instrument is capable of detecting analytes at the μg/L (or ppb) level. Using the similar conditions, the EPMM device was first tested and evaluated using a redox couple, $[Fe(CN)_6]^{3-}/[Fe(CN)_6]^{4-}$ to understand some of the basic voltammetric properties of the cell and the redox couple. The AC electrolysis was found to happen in the channel in accordance with other publishers like An[1] and Hayden.[10] However, this could not be the mechanism for the separation of ions in the channel. The concentration modulation due to AC electrolysis can be beneficial or detrimental depending on the AC modulation voltage and frequency. Further examination with the EPMM device was performed as experimented from the original journal published by Yoon.[2] Micro level trace metal ions were detected and attempted to separate. Our experiments showed that the detection is feasible but, separation was not modulated by the AC application. There could be an alternative, even better, yet unknown, mechanism for the separation observed in this study. This conclusion is based on the much narrower peak shape compared to that of the literature. Clearly further experiments must be done to examine these possibilities.

Another factor, i.e., the heat generated by the alternating currents or by the attenuation of the AC field applied to the side of the separation channel should be considered. According to An,[1] joule heating effect occurs when electric current flows through an electrically conductive fluid. As a result, a heat will be generated in the separation channel increasing the temperature of the system and therefore affecting the permittivity and conductivity. Therefore in the future, experimentally verifying whether joule heating is affecting the system should be examined. Implementing anti-heat or heat absorbent materials would be an option.

References

1. An, Ran, "Electrochemical Process in Microfluidic systems under AC electric Fields," Dissertation, Michigan Technological University, 2015. Http://digitalcommons.mtu.edu/etds/951.

2. Hui-Bog Noh, Pranjal Chandra, You-Jeong Kim, and Yoon-Bo Shim. "A Simple Separation Method with a Microfluidic Channel Based on Alternating Current Potential Modulation." Anal. Chem. 2012, 84, 9738-9744.

3. Jin Cui, Klaus Mathwig, Dileep Mampallil, and Serge G. Lemay. "Potential-Controlled Adsorption, Separation, and Detection of Redox Species in Nanofluidic Devies." Anal. Chem. 2018, 90, 7127-7130.

4. Max M Gong, Reza Nosrati, Maria C. San Gabriel, Armand Zini, and David Sinton. "Direct DNA Analysis with Paper-Based Ion Concentration Polarization." J. Am. Chem. Soc. 2015, 137, 13913-13919.

5. Min Zhou, Jeffrey E. Dick, Keke Hu, Michael V. Mirkin, and Allen J. Bard. "Ultrasensitive Electroanalysis: Femtomolar Determination of Lead, Cobalt, and Nickel." Anal. Chem. 2018, 90 (2), 1142-1146.

6. Qianwen Sun, Jikui Wang, Meihua Tang, Liming Huang, Zhiyi Zhang, Chang Liu, Xiaohua Lu, Kenneth W. Hunter, and Guosong Chen. "A New Electrochemical System Based on a Flow-Field Shaped Solid Electrode and 3D-Printed Thin-Layer Flow Cell: Detection of Pb^{2+} Ions by Voltammetry." Anal. Chem. 2017, 89 (9), 5024-5029.

7. Chauque, Susana & Oliva, Fabiana & Visintin, Arnaldo & Barraco Diaz, Daniel & Leiva, Ezequiel & Cámara, O.R.. (2017). Lithium titanate as anode material for lithium ion batteries: Synthesis, post-treatment and its electrochemical response. J. Electroanal. Chem. 799. 10.1016/j.jelechem.2017.05.052.

8. Allen J. Bard, Larry R. Faulkner. Electrochemical Methods Fundamentals and Applications. Austin, Texas, John Wiley & Sons, INC, 2001, Print.

9. S. J. Konopka and Bruce McDuffle. "Diffusion Coefficients of Ferri- and Ferrocyanide Ions in Aqueous Media Using Twin-Electrode Thin-Layer Electrochemistry." Anal. Chem. 1970, Vol. 42, No. 14. Pg 1741-1746.

10. Hayden, J. L. R., "Alternating-Current Electrolysis." Conference: Meeting of the American Institute of Electrical Engineers, New York, 1907: pg. 201.

11. V. N. Kiryushov, L. I. Skvortsova, and T. O Aleksandrova. "Electrochemical Behavior of the System Ferricynaide-Ferrocyanide at a Graphite-Epoxy Composite Electrode." J. Anal. Chem. 2011, Vol. 66. No. 5, pp. 510-514.

12. Chiun-Jye Yuan, Chung-Liang Wang, Teng Yang Wu, Kuo-Chu Hwang, Wei-Chi Chao. "Fabrication of a carbon fiber paper as the electrode and its application toward developing a sensitive unmediated amperometric biosensor." Biosensors and Bioelectronics 26 (2011) pp 2858-2863.

13. Victor H. Perez-Gonzales, Roberto C. Gallo-Villanueva, Braulio Cardenas-Benitez, Sergio O. Martinez-Chapa, and Blanca H. Lapizco-Encinas. "Simple Approach to Reducing Particle Trapping Voltage in Insulator-Based Dielectrophoretic systems." Anal. Chem. 2018, 90(7), pp 4310-4315.

14. Maria A. Komkova, Elena E. Karyakina, and Arkady A. Karyakin. "Noiseless Performance of Prussian Blue Based (Bio)sensors through Power Generation." Anal. Chem. 2017, 89(12), pp 6290-6294.

15. Robert L. Arechederra, Shelley D. Minteer. "Self-powered sensors." J. Bioanal. Chem. 2011, 400, pp 1605-1611.

16. A. Ramos, H. Morgan, N. G. Green, and A. Castellanos. "Ac electrokinetics: a review of forces in microelectrode structures." J. Phys. D: Appl. Phys. 31 (1998) pp 2338-2353.

17. Roger Parsons and M. A. V. Devanathan. "A General Thermodynamic Theory of the Ideal Polarized Electrode." Trans. Faraday Soc., 1953, 49, pp. 404-409.

18. David C. Grahame. "Entropy, Enthalpy and Free Energy of the Electrical Double Layer at an Ideal Polarized Electrode. Part I. Thermodynamic Theory." J. Phys. Chem. 16, 1117 (1948).

19. Paul Ruetschi and Pual Delahay. "Potential at zero charge for reversible and ideal polarized electrodes." J. Phys. Chem. 23, 697 (1955).

20. Jitendra Kumar and S. F. D'Souza. "Microbial biosensor for detection of methyl parathion using screen printed carbon electrode and cyclic voltammetry." J. Biosensors and Bioelectronics. Vol. 26. Issue. 11. (2011) pp 4289-4293.

21. J. Gonzalez, A. Molina, F. Martinez-Ortiz, M. Lopez-Tenes, R. G. Compton. "Analytical approach to the transient and steady state cyclic voltammetry of non-reversible electrode processes. Defining the transition from macro to microelectrodes." J. Electrochim Acta. Vol. 213 (2016) pp 911-926.

22. Daizong Ji, Lei Liu, Shuang Li, Chen Chen, Yanli Lu, Jiajia Wu, Qingjun Liu. "Smartphone-based cyclic voltammetry system with graphene modified screen printed electrodes for glucose detection." J. Biosensors and Bioelectronics. Vol. 98 (2017) pp 449-456.

23. Run-Xia He and Da-Wei Zha. "Cyclic voltammetry and voltabsorptometry studies of redox mechanism of lumazine." J. Electroanal. Chem. Vol. 791 (2017) pp 103-108.

24. Yuki Uchida, Enno Katelhon, Richard G. Compton. "Cyclic voltammetry with non-triangular waveforms: Electrochemically irreversible and quasi-reversible systems." J. Electroanal. Chem. Vol. 810 (2018) pp 135-144.

25. Miao-Rong Zhang and Ge-Bo Pan. "Porous GaN electrode for anodic stripping voltammetry of silver(I)." J. Talanta Vol. 165 (2017) pp 540-544.

26. Erick Flores, Jaime Pizarro, Fernando Godoy, Rodrigo Segura, Alejandra Gomez, Nicolas Agurto, Pamela Sepuveda. "An electrochemical sensor for the determination of Cu(II) using a modified electrode with ferrocenyl crwon ether compound by square wave anodic stripping voltammetry." J. Sensors and Actuators B: Chem. Vol. 251 (2017) pp 433-439.

27. Hussam, Abul. Chemistry 625 Lab; "Electrochemistry experiments: I) Cyclic Voltammetry (CV) and Square-Wave Voltammetry (SWV) of a Redox Couple. II)Anodic Stripping Voltammetry (ASV) Determination of Trace Metal Ions in Aqueous Samples. III) Double Potential Step Chronoamperometry and Chronocoulometry of $[Fe(CN)_6]^{3-}/[Fe(CN)_6]^{4-}$ System." George Mason University: Fairfax, VA, 2017.

28. L. K. Bieniasz. "A new theory of potential step chronoamperometry at hemispheroidal electrodes: Complete explicit semi-analytical formulae for the Faradaic current density and the Faradaic current." J. Eletroanal. Chem. Vol. 784 (2017) pp 91-101.

29. Jonathan C. Newland, Patrick R. Unwin, and Julie V. Macpherson. "Investigation of molecular partitioning between non polar oil droplets and aqueous solution

using double potential step chronoamperometry." J. Phys. Chem. 2014. 16. 10456.

30.   S. Seghir, N. Stein, C. Boulanger, and J. -M. Lecuire. "Electrochemical determination of the diffusion coefficient of cations into Chevrel phase-based electrochemical transfer junction by potential step chronoamperometry and impedance spectroscopy." J. Electrochim Acta (2010) Vol 56. No. 6. pp 2740-2747.

31.   M. Sadiku. "MEMS" IEEE Potentials Vol 21. No. 1. Pp 4-5.

32.   Richard S. Muller et al. Microelectromechanical Systems: Advanced Materials and Fabrication Methods. Washington, D.C., National Academy Press, 1997, Print.

33.   Packard, Corinne E., Murarka, Apoorva, Lam, Eric W., Schmidt, Martin A., Bulovic, Vladimir. "Contact-Printed Microelectromechanical Systems." J. Adv Mat (2010) Vol. 22 (16). Pp 1840-1844.

Biography

Sean J. Park graduated from W. T. Woodson High School, Fairfax, Virginia, in 2011. He Received his Bachelor of Arts from George Mason University in 2016 as a Chemist. He was then accepted to pursue his Master of Science in Chemistry and Biochemistry from the same university, George Mason. He held GTA position during all the academic years of Master's program along with conducting his own research under the supervision of Dr. Hussam. After successfully defending his research in the electrochemical/analytical topic, he received his Master of Science in Chemistry from George Mason University in 2019.